Geodynamic implications for zonal and meridional isotopic patterns across the northern Lau and North Fiji Basins

Journal Item

AGU PUBLICATIONS

Geochemistry, Geophysics, Geosystems

RESEARCH ARTICLE
10.1002/2016GC006651

Geodynamic implications for zonal and meridional isotopic patterns across the northern Lau and North Fiji Basins

Allison A. Price[1], Matthew G. Jackson[1], Janne Blichert-Toft[2], Mark D. Kurz[3], Jim Gill[4], Jerzy Blusztajn[3], Frances Jenner[5], Raul Brens[6], and Richard Arculus[7]

[1]Department of Earth Science, University of California, Santa Barbara, California, USA, [2]Laboratoire de Géologie de Lyon, CNRS UMR 5276, Ecole Normale Supériere de Lyon and Université Claude Bernard Lyon 1, Lyon, France, [3]Woods Hole Oceanographic Institution, Woods Hole, Massachusetts, USA, [4]Department of Earth Sciences, University of California, Santa Cruz, California, USA, [5]School of Environment, Earth and Ecosystems, Open University, Milton Keynes, UK, [6]Department of Earth and Planetary Sciences, Macquarie University, Sydney, New South Wales, Australia, [7]Research School of Earth Sciences, Australian National University, Canberra, ACT, Australia

Abstract We present new Sr-Nd-Pb-Hf-He isotopic data for 65 volcanic samples from the northern Lau and North Fiji Basins. This includes 47 lavas obtained from 40 dredge sites spanning an east-west transect across the Lau and North Fiji basins, 10 ocean island basalt (OIB)-type lavas collected from seven Fijian islands, and eight OIB lavas sampled on Rotuma. For the first time, we are able to map clear north-south and east-west geochemical gradients in $^{87}Sr/^{86}Sr$ across the northern Lau and North Fiji Basins: lavas with the most geochemically enriched radiogenic isotopic signatures are located in the northeast Lau Basin, while signatures of geochemical enrichment are diminished to the south and west away from the Samoan hot spot. Based on these geochemical patterns and plate reconstructions of the region, these observations are best explained by the addition of Samoa, Rurutu, and Rarotonga hot spot material over the past 4 Ma. We suggest that underplated Samoan material has been advected into the Lau Basin over the past ~4 Ma. As the slab migrated west (and toward the Samoan plume) via rollback over time, younger and hotter (and therefore less viscous) underplated Samoan plume material was entrained. Thus, entrainment efficiency of underplated plume material was enhanced, and Samoan plume signatures in the Lau Basin became stronger as the trench approached the Samoan hot spot. The addition of subducted volcanoes from the Cook-Austral Volcanic Lineament first from the Rarotonga hot spot, then followed by the Rurutu hot spot, contributes to the extreme geochemical signatures observed in the northeast Lau Basin.

Key Points:
- North-south and east-west geochemical gradients exist in the Lau and North Fiji Basins
- Underplated Samoan material has been entrained into the North Fiji and Lau Basins over the past ~4 Ma by toroidal flow
- Addition of subducted Cook-Austral Volcanic Lineament material also contributes to the extreme geochemical signatures in the Lau Basin

Supporting Information:
- Supporting Information S1
- Data Set S1
- Data Set S2
- Data Set S3

Correspondence to:
A. A. Price,
price@umail.ucsb.edu

Citation:
Price, A. A., M. G. Jackson, J. Blichert-Toft, M. D. Kurz, J. Gill, J. Blusztajn, F. Jenner, R. Brens, and R. Arculus (2017), Geodynamic implications for zonal and meridional isotopic patterns across the northern Lau and North Fiji Basins, *Geochem. Geophys. Geosyst.*, *18*, doi:10.1002/2016GC006651.

Received 19 OCT 2016
Accepted 7 FEB 2017
Accepted article online 11 FEB 2017

1. Introduction

Large-scale mantle convection releases heat from Earth's interior through three primary mechanisms: subduction, plate spreading at divergent boundaries, and buoyant mantle upwellings. There are only a few locations on Earth where expressions of these three mechanisms—arcs, back-arc spreading centers, and plumes—interact in close geographic proximity. The geographic juxtaposition of the upwelling Samoan plume, the Tonga Trench, and the associated back-arc ridges in the northern Lau and North Fiji Basins provides a rare natural laboratory where these systems interact intimately (Figure 1). While the effect of subduction and rollback-induced mantle flow on a nearby upwelling plume has been studied in a laboratory setting [e.g., *Druken et al*., 2011, 2014], it is critical to also evaluate this phenomenon in a natural setting.

The Tonga Trench—Samoan plume system provides an opportunity to evaluate mantle flow in the vicinity of a subducting slab experiencing rapid rollback (Figure 1). The unique geochemistry associated with the Samoan plume effectively acts as a geochemical tracer that can be followed as it infiltrates the depleted upper mantle of the Lau and North Fiji back-arc basins [e.g., *Druken et al*., 2014]. Tracking the shape and extent of the incursion of the Samoan material in the back-arc basins through geochemical analyses of lavas in the region can reveal how mantle flows around the nearby downgoing Tonga slab. Specifically, the Samoan plume is host to extreme isotopic signatures, including high $^{3}He/^{4}He$ (up to 33.8 Ra, where Ra is ratio to atmosphere, *Jackson et al*. [2007b]) and high $^{87}Sr/^{86}Sr$ (up to 0.721630, *Jackson et al*. [2007a]). Such signals are detectable in the nearby back-arc basins, even when highly diluted [e.g., *Druken et al*., 2014]. The

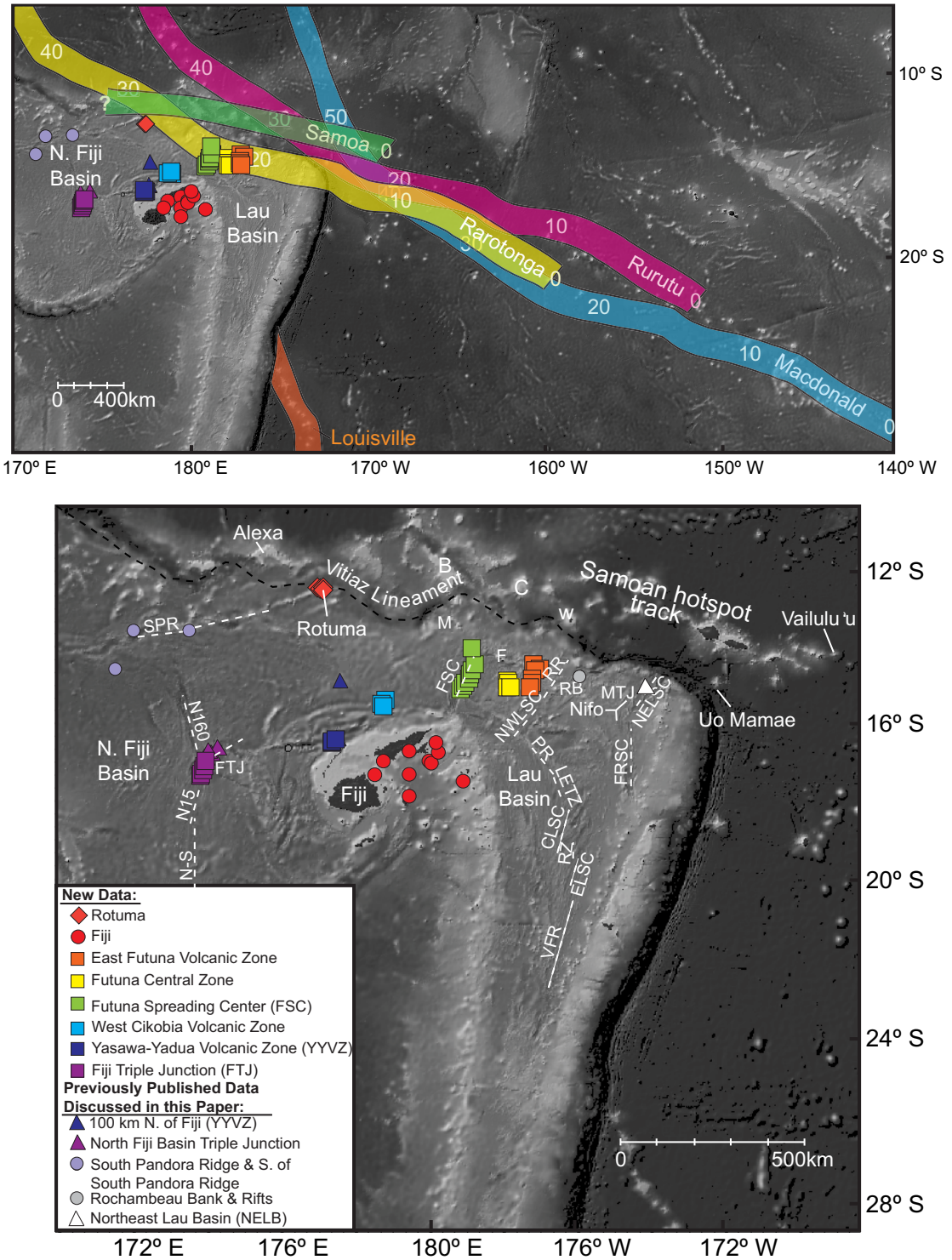

Figure 1. Map of the study region with locations of the samples from this study. Also shown with symbols are the locations of important, previously published data referenced in the text. Hot spot track reconstructions (and ages of the respective hot spot tracks, shown in millions of years) are based on *Wessel and Kroenke* [2008]. Abbreviations: B, *Bayonnaise Seamount*; C, *Combe Seamount*; W, *Wallis Island*; NELSC, *Northeast Lau Spreading Center*; FRSC, *Fonualei Rift and Spreading Center*; MTJ, *Mangatolu (King's) Triple Junction*; Nifo, *Niua fo'ou Island*, RB, *Rochambeau Bank*; RR, *Rochambeau Rifts*; NWLSC, *Northwest Lau Spreading Center*; PR, *Peggy Ridge*; LETZ, *Lau Extensional Transform Zone*; CLSC, *Central Lau Spreading Center*; RZ, *Relay Zone*; ELSC, *Eastern Lau Scpreading Center*; VFR, *Valu Fa Ridge*; F, *Futuna Island*; FSC, *Futuna Spreading Center*; M, *Manatu Seamount*; SPR, *South Pandora Ridge*; FTJ, *Fiji Triple Junction*. Base maps were created using GeoMapApp (http://www.geomapapp.org) with topographic and bathymetric data from SRTM_PLUS [*Becker et al.*, 2009].

detection of geochemical signatures with Samoan characteristics in the northern Lau and North Fiji back-arc basins has been used to evaluate the infiltration of Samoan mantle material around the northern edge of the subducting Pacific lithosphere [e.g., *Volpe et al*., 1988; *Gill and Whelan*, 1989; *Poreda and Craig*, 1992; *Wendt et al*., 1997; *Ewart et al*., 1998; *Pearce et al*., 2007; *Tian et al*., 2008, 2011; *Lupton et al*., 2009; *Hahm et al*., 2012; *Lytle et al*., 2012; *Price et al*., 2014, 2016; *Nebel and Arculus*, 2015].

With the exception of the Lau Basin and the Manus Basin [*Macpherson et al*., 1998], high $^{3}He/^{4}He$ ratios generally are not associated with back-arc basin lavas. Indeed, the lavas with elevated $^{3}He/^{4}He$ in the Manus Basin are associated with a mantle plume distinct from the Samoan plume [*French and Romanowicz*, 2015]. The observation of $^{3}He/^{4}He$ ratios of up to 28.1 Ra in the Lau Basin (at Rochambeau Rifts) represents a geochemical extreme among back-arc basins globally and has been suggested to relate to influence from the nearby Samoan plume [*Lupton et al*., 2009]. High $^{3}He/^{4}He$ ratios of this magnitude (i.e., 28.1 Ra) are uniquely associated with volcanic hot spots, and there are only four hot spots globally that have $^{3}He/^{4}He$ ratios as high or higher than that found at Rochambeau Rifts: Iceland [e.g., *Condomines et al*., 1983; *Kurz et al*., 1985; *Graham et al*., 1998; *Hilton et al*., 1999; *Moreira et al*., 2001; *Stuart et al*., 2003; *Macpherson et al*., 2005; *Starkey et al*., 2009; *Füri et al*., 2010], Hawaii [e.g., *Kurz et al*., 1982, 1983; *Valbracht et al*., 1997; *Mukhopadhyay et al*., 2003; *Keller et al*., 2004; *Garcia et al*., 2012], Galapagos [e.g., *Kurz and Geist*, 1999; *Graham et al*., 2003; *Jackson et al*., 2008; *Kurz et al*., 2009], and Samoa [*Farley et al*., 1992; *Workman et al*., 2004; *Jackson et al*., 2007b, 2014; *Hart and Jackson*, 2014]. Compared to the other potential high $^{3}He/^{4}He$ sources (Hawaii is ~4000 km from the 28.1 Ra locality in the northern Lau Basin, Galapagos ~9000 km and Iceland ~14,000 km), the Samoan hot spot is located near Rochambeau Rifts. Given the global rarity of localities with $^{3}He/^{4}He$ as high as that identified in the Lau Basin, it is unlikely that a second plume source (not yet identified) with $^{3}He/^{4}He$ as high as observed in Rochambeau Rifts is located in the Lau Basin, just ~800 km from the Samoan hot spot. Thus, Samoa is a likely contributor of the high $^{3}He/^{4}He$ signature in the Lau Basin. A key remaining question is the geographic extent over which the Samoan plume signature can be identified in the Lau and North Fiji Basins.

Several hot spot tracks in the southwest Pacific, near Samoa and the Lau Basin, have geochemically extreme isotopic signatures (e.g., HIMU [high-$\mu = {}^{238}U/{}^{204}Pb$] and EM1 [enriched mantle 1]), which influence the geochemistry of lavas in the Lau and North Fiji Basins [*Price et al*., 2016]. The Louisville, Rurutu, and Rarotonga hot spot tracks, and volcanoclastic sediments therefrom, have all been proposed to subduct into the Tonga Trench, and therefore have been argued to influence the geochemistry of back-arc lavas erupted in the vicinity of the subducting hot spot tracks [e.g., *Turner and Hawkesworth*, 1998; *Falloon et al*., 2007; *Regelous et al*., 2008; *Timm et al*., 2013; *Price et al*., 2016]. Fortunately, each of these subducted hot spots host geochemical signals distinctive from those found in Samoa and, in essence, act as additional tracers when introduced to the Lau and North Fiji Basins. Consequently, deconvolving the contributions of various geochemical plume signatures can constrain the origin of the geochemical signals in the Lau and North Fiji back-arc basin lavas and illuminate shallow mantle flow patterns in the region.

Here we use new isotopic data from lavas in the northern Lau and North Fiji Basins to further constrain the spatial distribution of geochemical signatures associated with the Samoa, Louisville, Rurutu, and Rarotonga hot spots. We present Hf, Pb, Sr, and Nd isotopic data from 65 samples spanning the Lau and North Fiji Basins; in addition to Hf, Pb, Sr, and Nd isotopic data, we also present new He isotopic data for a new suite of lavas from Rotuma and Fiji Islands. The majority of the samples discussed here come from the 2012 Northern Lau Transit Expedition of the R/V Southern Surveyor (cruise name: ss2012_v02). These lavas provide an east-west transect across the Lau and North Fiji Basins that gives an unprecedented new perspective on the distribution of geochemical signals in the region. Data for a new suite of ocean island basalt (OIB) lavas from Rotuma Island, located in the northern North Fiji Basin, as well as young, postarc OIB-type lavas from the Fijian Islands (i.e., Fijian ocean island basalt, FOIB, *Gill and Whelan* [1989]), complement this large data set.

The new data, in concert with previously published data from the region, show that geochemical patterns, both zonal and meridional, exist in the Lau and North Fiji Basins. These geochemical patterns reflect the geodynamic processes, including plume-slab interactions, that have operated over the past ~4 Ma as the back-arc basins have expanded in response to rapid rollback of the Tonga Trench near the upwelling Samoan mantle plume.

2. Geologic Background

2.1 Geologic Setting and Previous Work

Lavas erupted in back-arc basins globally are characterized by having geochemically depleted signatures [e.g., *McCulloch and Gamble*, 1991; *Langmuir et al*., 2006; *Pearce and Stern*, 2006]. However, the Lau Basin is unusual in that it samples several isotopically distinct hot spot components. First, the Samoan hot spot has been suggested to influence the geochemistry of Lau Basin lavas, where distinctive high-$^{87}Sr/^{86}Sr$ and high-$^{3}He/^{4}He$ signatures—associated with the Samoan plume—have been identified in the Rochambeau Rifts in the northern Lau Basin [e.g., *Lytle et al*., 2012; *Lupton et al*., 2009; *Poreda and Craig*, 1992] (Figure 1). The Samoan hot spot track, constructed on >100 Ma Pacific lithosphere [*Müller et al*., 2008], extends west of the Samoan hot spot (Figure 1). The hot spot track runs parallel to (and slightly north of) the Vitiaz Lineament, a bathymetric low (Figure 1) that defines the boundary between the old, thick Pacific lithosphere and the young, thin lithosphere of the Lau and North Fiji Basins.

A keel of underplated Samoan plume residue, attached to the base of the lithosphere, is suggested to be present along the length of the Samoan hot spot, including the portion of the hot spot that lies north of the Lau and North Fiji Basins [*Price et al*., 2014]. *Price et al*. [2014] argued that rollback of the subducting Pacific Plate, from ~4 Ma to present, has induced a long-lived toroidal flow field around the northern edge of the subducting Tonga slab: underplated Samoan plume material is entrained in the toroidal flow field and advected southward into the Lau and North Fiji Basins [*Price et al*., 2014], thus explaining the Samoan plume signatures—including high $^{3}He/^{4}He$ and enriched $^{87}Sr/^{86}Sr$—in the Lau and North Fiji Basins up to 1400 km west of the Samoan hot spot. Additionally, underplated plume material will have a tendency to flatten and spread laterally at the base of the oceanic lithosphere, which may help transport Samoan plume material southward to the northern Lau and North Fiji Basins [*Phipps-Morgan et al*., 1995]. Thus, together with any southward advection due to slab-induced toroidal flow, the lateral spreading due to pancaking of the plume will help mobilize the plume keel to the south and into the northern Lau and North Fiji Basins.

An additional possible contributor to the geochemical diversity in the southern Lau Basin is the Louisville hot spot, which currently subducts into the Tonga trench at ~26°S, but lies outside of the area considered in this study (see Figure 1). The Louisville hot spot exhibits relatively high $^{206}Pb/^{204}Pb$ (up to 19.6060, *Vanderkluysen et al*. [2015]) and $^{208}Pb/^{204}Pb$ (up to 39.3695, *Beier et al*. [2011], when considering only relatively fresh lavas) and has been suggested to contribute to the elevated Pb isotopic compositions observed in a subset of volcanoes from both the northern [e.g., *Turner and Hawkesworth*, 1998; *Ewart et al*., 1998] and southern [e.g., *Timm et al*., 2013] Tonga arc. However, geochemical signatures associated with the Louisville hot spot have not been detected in the region of the northern Lau back-arc basin that, together with the North Fiji Basin, is the focus of this study [*Price et al*., 2016]. Lastly, the subduction of seamounts from the Cook-Austral Volcanic Lineament [*Falloon et al*., 2007; *Todd et al*., 2009], in particular volcanoes associated with the Rarotonga and Rurutu hot spots, influence the geochemistry of Lau Basin lavas [*Price et al*., 2016]. Based on plate reconstructions [*Wessel and Kroenke*, 2008], the Rarotonga hot spot, which exhibits EM1 isotopic signatures, subducts into the northern Tonga Trench beneath the northeast Lau Basin (Figure 1). The same plate reconstructions show that the Rurutu hot spot, which hosts HIMU signatures, also likely subducts into the northernmost Tonga Trench (Figure 1). Furthermore, extreme geochemical enrichment of lavas from the northeast Lau Basin, including the most radiogenic Pb (HIMU) isotopic ratios and the most enriched $^{143}Nd/^{144}Nd$ (EM1) signatures in the region, can be linked to the subduction of the HIMU Rurutu hot spot track and the EM1 Rarotonga hot spot track, respectively. In conclusion, up to three hot spots originating in the South Pacific superswell influence the geochemistry of the northern Lau and North Fiji Basins, either by toroidal advection of underplated plume material (Samoa) or by subduction of older portions of hot spot tracks (Rarotonga and Rurutu).

2.2. Sample Locations

The locations of the new samples presented in this study are shown in Figure 1 and Table 1. The 47 dredged lavas, from 40 dredge localities in the Lau and North Fiji Basins, were collected during the 2012 cruise of the R/V Southern Surveyor, expedition SS_V02; all samples have the prefix NLTD (Northern Lau Transect Dredges). We do not present new ages on the lavas in this study. However, the dredging campaign exclusively targeted ridge segments, and the visually fresh appearance of the volcanic glasses is consistent with young sample ages. We divide these lavas into six geographic groups, listed from East to West: East Futuna

Table 1. Sr, Nd, Hf. and Pb Isotopic Analyses on Northern Lau Basin and North Fiji Basin Lavas

Sample Location	Sample Name	Lat.	Lon.	$^{176}Hf/^{177}Hf$[a]	Error (2σ)[b]	εHf[c]	$^{87}Sr/^{86}Sr$[a]	Error (2σ)[b]	$^{143}Nd/^{144}Nd$[a]	Error (2σ)[b]	εNd[c]	$^{206}Pb/^{204}Pb$[a]	Error (2σ)[b]	$^{207}Pb/^{204}Pb$[a]	Error (2σ)[b]	$^{208}Pb/^{204}Pb$[a]	Error (2σ)[b]	$\Delta^{208}Pb/^{204}Pb$	$\Delta^{207}Pb/^{204}Pb$
Northern Lau Transect Dredges (NLTD)																			
Fiji Triple Junction	NLTD 44-1	−17.31	173.80	0.283278	8	17.9	0.702910	8	0.513129	4	9.6	18.0671	9	15.4760	8	37.8191	20	34.9	2.7
Fiji Triple Junction	NLTD 45-1	−17.19	173.85	0.283051	3	9.9	0.703621	6	0.512850	10	4.1	18.6162	5	15.5731	4	38.6790	5	54.5	6.4
Fiji Triple Junction	NLTD 45-2	−17.19	173.85	0.283304	4	18.8	0.702908	5	0.513150	11	10.0	18.0582	15	15.4784	12	37.8207	34	36.1	3.0
Fiji Triple Junction	NLTD 46-1	−17.07	173.89	0.283307	3	18.9	0.702850	12	0.513145	20	9.9	18.0090	11	15.4763	9	37.7408	17	34.1	3.3
Fiji Triple Junction	NLTD 39-5	−16.94	173.93	0.283255	3	17.1	0.703108	4	0.513030	13	7.6	18.2272	18	15.5058	19	38.0823	50	41.9	3.9
Fiji Triple Junction	NLTD 40-1	−17.31	173.80	0.283023	3	8.9	0.703728	11	0.512855	6	4.2	18.6846	19	15.5861	14	38.7977	41	58.1	7.0
Fiji Triple Junction	NLTD 41-8	−16.95	173.92	0.283049	2	9.8	0.703648	29	0.512874	14	4.6	18.6273	8	15.5738	8	38.7000	24	55.3	6.4
Fiji Triple Junction	NLTD 42-1	−16.98	173.92	0.283094	3	11.4	0.703561	16	0.512925	15	5.6	18.5829	25	15.5666	15	38.6258	48	53.2	6.1
Fiji Triple Junction	NLTD 43-1	−16.98	173.91	0.283313	4	19.1	0.702883	5	0.513140	14	9.8	18.0296	28	15.4661	23	37.7730	39	34.8	2.1
Fiji Triple Junction	NLTD 49-1	−16.95	173.92	0.283304	3	18.8	0.702914	27	0.513140	17	9.8	18.0106	33	15.4728	23	37.7733	60	37.2	2.9
Fiji Triple Junction	NLTD 50-1	−16.96	173.94	0.283284	3	18.1	0.702973	43				18.0405	27	15.4798	26	37.8063	58	36.8	3.3
Fiji Triple Junction	NLTD 50-2	−16.96	173.94	0.283134	3	12.8	0.703490	27	0.512983	24	6.7	18.4810	14	15.5477	16	38.4782	36	50.8	5.3
Fiji Triple Junction	NLTD 50-3	−16.96	173.94	0.283157	2	13.6	0.703480	7	0.512959	4	6.3	18.4829	17	15.5480	16	38.4771	44	50.4	5.3
Fiji Triple Junction	NLTD 47-2	−16.85	173.96	0.283291	3	18.3	0.702898	5				18.0333	14	15.4710	14	37.7793	45	35.0	2.5
Fiji Triple Junction	NLTD 47-3	−16.85	173.96	0.283298	4	18.6	0.702902	4	0.513085	8	8.7	18.1458	22	15.4935	13	37.9333	35	36.8	3.6
Fiji Triple Junction	NLTD 48-1	−16.88	173.92	0.283039	3	9.4	0.703671	17	0.512883	7	4.8	18.6409	11	15.5747	10	38.7198	26	55.6	6.3
Yasawa-Yadua Volcanic Zone	NLTD 2-4	−16.39	177.33	0.283309	2	19.0	0.703662	24	0.513125	10	9.5	18.5649	3	15.5405	2	38.4264	5	35.4	3.7
Yasawa-Yadua Volcanic Zone	NLTD 3-6	−16.45	177.34	0.283273	5	17.7	0.704024	7	0.512992	6	6.9	18.6705	6	15.5597	7	38.5138	24	31.4	4.5
Yasawa-Yadua Volcanic Zone	NLTD 4-2	−16.43	177.43	0.283370	2	21.1	0.703175	22	0.513172	8	10.4	18.4516	23	15.5161	34	38.2973	110	36.2	2.5
Yasawa-Yadua Volcanic Zone	NLTD 36-2	−16.43	177.34	0.283339	2	20.1	0.703717	3	0.513105	10	9.1	18.5401	31	15.5373	19	38.3891	72	34.7	3.7
Yasawa-Yadua Volcanic Zone	NLTD 36-7	−16.43	177.34	0.283356	2	20.6	0.703353	5	0.513120	9	9.4	18.5321	4	15.5347	3	38.3927	8	36.0	3.5
West Cikobia	NLTD 7-12	−15.43	178.75	0.283129	3	12.6	0.703738	22	0.512921	11	5.5	18.6159	4	15.5685	2	38.6065	7	47.3	6.0
West Cikobia	NLTD 8-1	−15.46	178.71	0.283178	4	14.4	0.703523	43	0.513013	13	7.3	18.4872	42	15.5363	45	38.4127	101	43.5	4.1
West Cikobia	NLTD 9-1	−15.53	178.73	0.283225	9	16.0	0.703538	38	0.512963	24	6.3	18.7070	6	15.6167	5	38.8015	14	55.8	9.8
West Cikobia	NLTD 35-3	−15.36	178.79	0.283207	2	15.4	0.703396	8	0.512941	11	5.9	18.6267	17	15.5766	21	38.6452	64	49.8	6.6
Futuna Spreading Center	NLTD 10-2	−14.85	−179.02	0.283221	2	15.9	0.703542	25	0.512970	13	6.5	18.5458	36	15.5367	30	38.4489	72	40.0	3.5
Futuna Spreading Center	NLTD 11-1	−14.82	−178.98	0.283109	3	11.9	0.703506	8	0.512936	4	5.8	18.7078	7	15.5409	6	38.5755	16	33.1	2.2
Futuna Spreading Center	NLTD 12-2	−14.59	−178.87	0.283191	3	14.8	0.703449	22	0.512971	13	6.5	18.6469	15	15.5395	15	38.5639	48	39.3	2.7
Futuna Spreading Center	NLTD 13-2	−14.42	−178.80	0.283174	5	14.2	0.703469	7	0.513018	10	7.4	18.4591	30	15.5275	21	38.3211	51	37.7	3.6
Futuna Spreading Center	NLTD 14-1	−14.71	−178.93	0.283186	3	14.6	0.703557	8	0.512960	15	6.3	18.6365	12	15.5628	14	38.5962	39	43.8	5.2
Futuna Spreading Center	NLTD 28-20	−14.00	−178.88	0.283022	4	8.8	0.703597	10	0.512862	5	4.4	18.4382	8	15.4999	7	38.2966	10	37.8	1.0
Futuna Spreading Center	NLTD 30-24	−15.01	−179.11	0.283160	2	13.7	0.703443	6											
Futuna Spreading Center	NLTD 30-38	−15.01	−179.11	0.283155	3	13.6	0.703478	12	0.512982	8	6.7	18.5670	25	15.5358	24	38.4612	72	38.7	3.2
Futuna Spreading Center	NLTD 31-11	−14.99	−179.13	0.283170	4	14.1	0.703625	7	0.512891	12	4.9	18.7438	22	15.5745	20	38.6697	59	38.1	5.2

AGU Geochemistry, Geophysics, Geosystems

10.1002/2016GC006651

Table 1. (continued)

Sample Location	Sample Name	Lat.	Lon.	$^{176}Hf/^{177}Hf$[a]	Error (2σ)[b]	εHf[c]	$^{87}Sr/^{86}Sr$[a]	Error (2σ)[b]	$^{143}Nd/^{144}Nd$[a]	Error (2σ)[b]	εNd[c]	$^{206}Pb/^{204}Pb$[a]	Error (2σ)[b]	$^{207}Pb/^{204}Pb$[a]	Error (2σ)[b]	$^{208}Pb/^{204}Pb$[a]	Error (2σ)[b]	$\Delta^{208}Pb/^{204}Pb$	$\Delta^{207}Pb/^{204}Pb$
Futuna Spreading Center	NLTD 32-1	−14.97	−179.11	0.283148	3	13.3	0.703568	8	0.512960	8	6.3	18.7181	11	15.5700	8	38.6742	28	41.7	5.0
Futuna Spreading Center	NLTD 33-7	−15.05	−179.18	0.283191	3	14.8	0.703494	4	0.512954	15	6.2	18.6028	6	15.5479	5	38.5079	23	39.0	4.0
Futuna Central Zone	NLTD 22-14	−14.89	−177.90	0.283132	2	12.7	0.703747	8	0.512949	15	6.1	18.4822	15	15.5391	15	38.3526	48	38.1	4.5
Futuna Central Zone	NLTD 23-12	−14.92	−177.90	0.283194	3	14.9	0.703489	4	0.513030	4	7.6								
Futuna Central Zone	NLTD 24-1	−15.03	−177.83	0.283147	3	13.3	0.703660	7	0.512950	5	6.1	18.5036	6	15.5476	7	38.4059	17	40.8	5.1
Futuna Central Zone	NLTD 26-7	−15.03	−177.92	0.283154	4	13.5	0.703826	9	0.512943	10	5.9	18.5147	8	15.5404	9	38.4280	31	41.7	4.2
Futuna Central Zone	NLTD 16-1	−14.62	−177.90	0.283125	2	12.5	0.703667	3	0.512941	7	5.9								
East Futuna Volcanic Zone	NLTD 15-1	−14.44	−177.21	0.283154	2	13.5	0.703666	8	0.512970	5	6.5	18.2742	7	15.4987	6	38.1384	17	41.8	2.7
East Futuna Volcanic Zone	NLTD 17-1	−14.54	−177.02	0.283136	3	12.9	0.703797	33	0.512936	7	5.8	18.5538	12	15.5364	17	38.4039	16	34.5	3.4
East Futuna Volcanic Zone	NLTD 18-1	−14.92	−177.25	0.283223	4	16.0	0.703631	13	0.513041	14	7.9	18.3801	10	15.5367	8	38.2610	19	41.2	5.3
East Futuna Volcanic Zone	NLTD 18-3	−14.92	−177.25	0.283207	2	15.4	0.703682	9	0.513021	10	7.5	18.4819	11	15.5534	13	38.3808	34	40.9	5.9
East Futuna Volcanic Zone	NLTD 19-16	−14.80	−177.24	0.283169	3	14.1	0.703805	33	0.512959	19	6.3	18.6365	17	15.5556	9	38.5123	28	35.4	4.4
East Futuna Volcanic Zone	NLTD 21-1	−15.00	−177.29	0.283248	2	16.8	0.703518	14	0.513083	22	8.7	18.3585	2	15.5207	3	38.2412	8	41.9	4.0
Fiji Lavas																			
Fiji (Koro, Type I FOIB)	W251	−17.31	179.44	0.283057	4	10.1	0.703670	8	0.512877	5	4.7	18.7242	6	15.5644	5	38.4382	13	17.4	4.4
Fiji (Mago, Type I FOIB)	Mago	−17.46	−179.15	0.283045	4	9.7	0.703633	8	0.512861	4	4.4	18.7755	5	15.5838	5	38.5026	14	17.6	5.8
Fiji (Nairai, Type I FOIB)	WQ271a	−17.84	179.41	0.283054	3	10.0	0.703627	10	0.512888	4	4.9	18.7343	7	15.5678	6	38.4642	14	18.7	4.6
Fiji (Taveuni, Type I FOIB)	WQ64	−16.75	−179.86	0.283079	6	10.9	0.703731	11	0.512881	4	4.7	18.7870	12	15.5736	10	38.5343	26	19.4	4.6
Fiji (Taveuni, Type I FOIB)	W135	−16.50	−179.90	0.283142	5	13.1	0.703496	11	0.512946	4	6.0								
Fiji (Taveuni, Type I FOIB)	FJ-12-3	−17.00	179.93	0.283096	4	11.5	0.703651	8	0.512922	6	5.5	18.7568	7	15.5766	6	38.5096	14	20.6	5.2
Fiji (Taveuni, Type I FOIB)	FJ-12-5	−16.96	179.91	0.283073	5	10.6	0.703691	10	0.512889	5	4.9	18.7927	11	15.5779	10	38.5411	23	19.4	5.0
Fiji (Vatu-i-ra, Type I FOIB)	WQ208	−17.32	178.47	0.283041	5	9.5	0.703807	10	0.512877	5	4.7	18.8700	6	15.5830	5	38.6959	13	25.5	4.6
Fiji (Suvasuva, Type I/II FOIB)	WQ28	−16.76	179.38	0.283022	6	8.8	0.704071	10	0.512819	4	3.5	18.8022	9	15.6015	8	38.5928	18	23.4	7.2
Fiji (Seatura, Type II FOIB)	WQ7b	−17.00	178.71	0.282994	5	7.9	0.703926	8	0.512831	4	3.8	18.5540	7	15.5712	6	38.5055	15	44.7	6.9
Rotuma Lavas																			
Rotuma, Oinafa Basalt 2	ROT-3	−12.49	177.02	0.283152	4	13.4	0.703590	10	0.512974	5	6.6	18.8831	6	15.5606	5	38.6401	12	18.3	2.3
Rotuma, Oinafa Basalt 1	ROT-4	−12.51	177.04	0.283147	5	13.3	0.703517	10	0.512988	6	6.8	18.8449	6	15.5701	5	38.5608	11	15.0	3.6
Rotuma, Oinafa Basalt 2	ROT-6	−12.52	177.09	0.283141	5	13.0	0.703574	10	0.512951	5	6.1	18.8524	5	15.5610	5	38.6136	11	19.4	2.6
Rotuma, Oinafa Basalt 1	ROT-8	−12.51	177.14	0.283132	5	12.7	0.703602	11	0.512949	4	6.1	18.8980	8	15.5709	6	38.6531	16	17.8	3.1
Rotuma, Oinafa Basalt 2	ROT-11	−12.48	177.09	0.283134	4	12.8	0.703646	8	0.512946	5	6.0	18.8739	6	15.5678	5	38.6406	12	19.5	3.1
Rotuma, Oinafa Basalt 2	ROT-12	−12.48	177.09	0.283133	4	12.8	0.703632	10	0.512944	3	6.0	18.8723	19	15.5691	7	38.6424	23	19.9	3.2
Rotuma, Oinafa Basalt 1	ROT-13	−12.48	177.06	0.283129	7	12.6	0.703539	10	0.512962	4	6.3	18.8583	7	15.5640	6	38.5959	14	16.9	2.9
Rotuma, Oinafa Basalt 1	ROT-15	−12.51	177.01	0.283139	5	13.0	0.703564	10	0.512953	4	6.1	18.8806	7	15.5608	6	38.6461	15	19.2	2.3
USGS Reference Materials																			
Reference Material	AGV-2-1 (This Study)[d,e]											18.8633	16	15.6132	13	38.5282	35	9.5	7.7
Reference Material	AGV-2-2 (This Study)[d,e]											18.8688	8	15.6135	9	38.5343	27	9.5	7.7

AGU Geochemistry, Geophysics, Geosystems

10.1002/2016GC006651

Table 1. (continued)

Sample Location	Sample Name	Lat.	Lon.	$^{176}Hf/^{177}Hf$[a]	Error (2σ)[b]	εHf[c]	$^{87}Sr/^{86}Sr$[a]	Error (2σ)[b]	$^{143}Nd/^{144}Nd$[a]	Error (2σ)[b]	εNd[c]	$^{206}Pb/^{204}Pb$[a]	Error (2σ)[b]	$^{207}Pb/^{204}Pb$[a]	Error (2σ)[b]	$^{208}Pb/^{204}Pb$[a]	Error (2σ)[b]	$\Delta^{208}Pb/^{204}Pb$	$\Delta^{207}Pb/^{204}Pb$
Reference Material	AGV-2-3 (This Study)[d,e]											18.8661	19	15.6125	19	38.5294	57	9.3	7.6
Reference Material	AGV-2-4 (This Study)[d,e]											18.8683	20	15.6137	21	38.5339	58	9.5	7.7
Reference Material	AGV-2-5 (This Study)[d,e]											18.8681	8	15.6128	8	38.5325	32	9.4	7.6
Reference Material	AGV-2-6 (This Study)[d,e]						0.703977	10	0.512765	17		18.8653	5	15.6129	5	38.5319	14	9.7	7.7
Reference Material	AGV-2-6 rep (This Study)[d,e]						0.703984	11	0.512771	7		18.8699	8	15.6160	6	38.5416	20	10.1	7.9
Reference Material	AGV-2-7 (This Study)[d,e]						0.703976	11	0.512790	10		18.8653	8	15.6130	8	38.5323	21	9.7	7.7
Reference Material	AGV-2-7 rep (This Study)[d,e]						0.703989	8				18.8681	8	15.6139	8	38.5354	32	9.7	7.8
Reference Material	AGV-2-8 (This Study)[d,e]						0.703980	14	0.512793	11		18.8650	4	15.6126	5	38.5312	17	9.6	7.7
Reference Material	AGV-2-8 rep (This Study)[d,e]						0.703990	11	0.512792	11		18.8677	3	15.6136	3	38.5346	10	9.6	7.7
Reference Material	AGV-2-9 (This Study)[d,e]						0.703976	13	0.512783	6		18.8652	6	15.6128	6	38.5321	16	9.7	7.7
Reference Material	AGV-2-9 rep (This Study)[d,e]						0.703971	8				18.8671	8	15.6133	9	38.5343	27	9.7	7.7
Reference Material	AGV-2 (This Study)[d,e]			0.282989	4	7.7	0.703995	8	0.512774	5	2.7	18.8660	9	15.6174	9	38.5299	32	9.4	8.1
Reference Material	AGV-2 Average this study[b]						0.703982	16	0.512781	22		18.8667	36	15.6137	28	38.5330	65		
Reference Material	AGV-2 (data from *Weis et al.* [2006, 2007])[b,d]			0.282987	9	7.6	0.703973	9	0.512779	10	2.8	18.8692	63	15.6186	71	38.5488	135	10.9	8.2
Reference Material	BCR-2-1 (This Study)[d,e]											18.7527	9	15.6196	10	38.7190	41	42.0	9.6
Reference Material	BCR-2-2 (This Study)[d,e]											18.7436	14	15.6186	8	38.6975	29	40.9	9.6
Reference Material	BCR-2-3 (This Study)[d,e]											18.7558	7	15.6192	5	38.7249	19	42.2	9.5
Reference Material	BCR-2-4 (This Study)[d,e]											18.7580	10	15.6195	8	38.7298	25	42.4	9.5
Reference Material	BCR-2-5 (This Study)[d,e]			0.282882	4		0.705000	14	0.512634	7		18.7556	2	15.6200	2	38.7250	21	42.2	9.6
Reference Material	BCR-2-5 rep (This Study)[d,e]											18.7582	12	15.6209	10	38.7286	24	42.3	9.7
Reference Material	BCR-2-6 (This Study)[d,e]			0.282884	5		0.705001	6	0.512622	8		18.7531	5	15.6195	5	38.7244	21	42.5	9.6
Reference Material	BCR-2-6 rep (This Study)[d,e]						0.705000	10	0.512623	9		18.7600	18	15.6230	18	38.7354	74	42.8	9.8
Reference Material	BCR-2-7 (This Study)[d,e]						0.705004	16	0.512636	13		18.7563	12	15.6206	10	38.7279	24	42.5	9.6
Reference Material	BCR-2-7 rep (This Study)[d,e]						0.705006	11	0.512619	4		18.7583	7	15.6211	6	38.7301	16	42.4	9.7
Reference Material	BCR-2-8 (This Study)[d,e]						0.705013	6	0.512615	9		18.7555	7	15.6198	8	38.7255	27	42.3	9.6
Reference Material	BCR-2-8 rep (This Study)[d,e]											18.7582	9	15.6209	10	38.7288	41	42.3	9.6
Reference Material	BCR-2 (This Study)[d,f]			0.282886	5	4.0	0.704989	10	0.512630	5	−0.2	18.7558	9	15.6251	8	38.7414	22	43.9	10.1
Reference Material	BCR-2 Average this study[b]			0.282884	4		0.705002	15	0.512626	16		18.7555	83	15.6206	35	38.7260	204		
Reference Material	BCR-2 (data from *Weis et al.* [2006. 2007])[b,d]			0.282873	8	3.6	0.705005	10	0.512627	12	−0.2	18.7533	195	15.6262	40	38.7282	405	42.8	10.2

[a]Nd isotopic compositions are corrected to the La Jolla value of 0.511847 (which, when converted using *Tanaka et al.*'s [2000] La Jolla to JNdi-1, is equivalent to a JNdi-1 value of 0.512104). Sr isotopic compositions are corrected to the NBS 987 value of 0.710240. Pb isotopic compositions are corrected to the NIST 981 values of *Eisele et al.* [2003] ($^{206}Pb/^{204}Pb = 16.9409$, $^{207}Pb/^{204}Pb = 15.4976$, and $^{208}Pb/^{204}Pb = 36.7262$). The unweighted mean $^{176}Hf/^{177}Hf$ of the JMC-475 Hf standard run alternately with the samples were identical within error to the preferred value of 0.282163 ± 0.000009 [*Blichert-Toft et al.*, 1997], hence no corrections were applied to the $^{176}Hf/^{177}Hf$ data.

[b]Error is 2σ standard error of the mean, and is absolute (not relative), and are for the last digits of the reported isotopic ratio. Errors represent internal (in-run) precision. However, for the average values reported for AGV-2 and BCR-2 from this study and the *Weis et al.* [2006, 2007] studies, the error reported represents the 2 standard deviation of the mean of the individual reference material analyses.

[c]The Nd and Hf epsilon notations were calculated using the CHUR values of $^{143}Nd/^{144}Nd = 0.512638$ *Jacobsen and Wasserburg* [1980] and *Hamilton et al.* [1983] and $^{176}Hf/^{177}Hf = 0.282772$ [*Blichert-Toft and Albarède*, 1997].

[d]The isotopic compositions of the USGS reference materials analyzed in this study are reported together with the isotopic compositions reported in *Weis et al.* [2006, 2007]. Note that the results from the *Weis et al.* [2006, 2007] studies have been renormalized to the preferred Sr, Nd, Hf, and Pb-isotopic compositions for NBS 987, JNdi-1 (and the *Tanaka et al.* [2000] conversion for JNdi-1 to La Jolla), JMC475 and NBS 981, respectively, that we use in this study. Note that the errors reported for the *Weis et al.* [2006, 2007] values represent 2 standard deviation of multiple measurements of the same standard.

[e]Reference material was run with samples from *Price et al.* [2014] and NLTD samples from this study, using identical chemical separation protocols and mass spectrometry; all of the data reported on these reference materials were presented in *Price et al.* [2014]. Note that in this study the Pb isotopic ratios here are normalized to *Eisele et al.* [2003], which differs from the normalization in *Price et al.* [2014]. Each sample represents a separate, ~200 mg aliquot of powder that was dissolved and processed separately through column chemistry. Over the course of this study, eight separate aliquots of BCR-2 and nine separate aliquots of AGV-2 were dissolved and processed separately through column chemistry. Samples with "rep" are replicate runs of the same sample dissolution, but run during a different analytical session on the MC-ICP-MS at WHOI.

[f]Reference material was run with samples from *Price et al.* [2016] and the Fiji/Rotuma samples from this study, using identical chemical separation protocols and mass spectrometry; the Hf and Pb isotopic data for these reference materials were published previously in *Price et al.* [2016] and the Sr and Nd isotopic data are published here.

AGU Geochemistry, Geophysics, Geosystems

10.1002/2016GC006651

Volcanic Zone, Futuna Central Zone, Futuna Spreading Center, West Cikobia Volcanic Zone, the Yasawa-Yadua Volcanic Zone, and the Fiji Triple Junction (Figure 1).

Samples from Rotuma Island were collected by A. Price during the 2013 field season. The eight rocks analyzed here sample the two known basalt units on the island: Oinafa Basalt 1 (0.1–0.2 Ma) and Oinafa Basalt 2 (<15,000 years) [*Woodhall*, 1987].

The 10 Fijian OIB samples were taken from seven different Fijian Islands: Suvasuva (sample WQ28, 2.65 ± 0.22 Ma, *Whelan et al*. [1985]), Koro (sample W251, 1.27 ± 0.15 Ma, *Whelan et al*. [1985]), Vatu-i-ra (sample WQ208, 2.72 ± 0.34 Ma, *Whelan et al*. [1985]), Mago (sample "Mago"), Seatura (sample WQ7b), Nairai (sample WQ271a, 0.11 ± 0.03 Ma, *Whelan et al*. [1985]), and Taveuni (samples FJ-12-3, FJ-12-5, WQ64, and W135, the last of which has an age of 0.74 ± 0.09 Ma, *Whelan et al*. [1985]). Ages are not available for all of the individual samples presented here, but Fijian OIB lavas have been shown to have ages that post-date arc volcanism at Fiji (<3 Ma; *Gill and Whelan* [1989]). Most Fijian samples were provided by J. Gill, but two samples (FJ-12-3 and FJ-12-5) were collected on Taveuni Island by A. Price during the 2012 field season. Some isotopic, major and trace element data were reported previously by *Gill* [1984], *Gill and Whelan* [1989], and *Pearce et al*. [2007], and we augment these data sets here.

3. Methods

3.1. Major Element Analyses

Samples were fused with di-lithium tetraborate in graphite crucibles using a Nabertherm furnace at UCSB. Major element analyses of the fused sample beads were determined for five Fiji and eight Rotuma Island OIB samples and three USGS reference materials by X-ray fluorescence (XRF) at Pomona College. Analytical and data reduction methods followed those outlined in *Lackey et al*. [2012]. The new Fijian OIB and Rotuma major element data are summarized in supporting information Data Set 1, together with previously published data on these lavas and data for aliquots of BHVO-2, AGV-2, and BCR-2 USGS reference materials that were run (as unknowns) during the same sample preparation and analytical sessions as the Fiji OIB and Rotuma samples (see supporting information Data Set 1). Previously published XRF major element data for the remaining five Fijian rocks examined here are reported in *Gill and Whelan* [1989] (see supporting information Data Set 1).

3.2. Trace Element Analyses

Trace element concentrations of most Fiji and all Rotuma lavas examined in this study were measured by ICP-MS at Washington State University (WSU) on ~200 mg of whole rock powders that were prepared in an Spex alumina ceramic mill at UCSB. The data are reported in supporting information Data Set 2 together with data for a ~200 mg aliquot of BCR-2 that was run (as an unknown) during the same analytical session as the five Fiji and five Rotuma lavas. The precision for the ICP-MS analyses at WSU is 0.77–3.2% (1σ) for all elements except Th (9.5%) and U (9.3%) [*Knaack et al*., 1994; *Hart and Blusztajn*, 2006]. Trace element concentrations for two Fijian samples (samples W251 and W271a) were measured by ICP-MS at UCSC following the methods of *Tollstrup et al*. [2010] and are reported here for the first time. Two additional Fijian lavas examined in this study were previously characterized for trace element compositions by ICP-MS (samples WQ28 and WQ7b from *Pearce et al*. [2007]) (supporting information Data Set 2).

3.3. Hf, Pb, Sr, and Nd Chemical Separation and Mass Spectrometry

All Hf, Pb, Sr, and Nd isotopic measurements presented in this study were undertaken on 200–450 mg of fresh volcanic glass (for NLTD lavas) or whole rock chips (for Fiji and Rotuma lavas). Different methods of sample leaching, dissolution, column separation, and mass spectrometric analysis were used when analyzing the NLTD samples (Fall 2012–Spring 2013) and samples from Rotuma and Fiji Islands (Fall 2014–Spring 2015). These methods are described below.

All samples were acid leached prior to digestion at the Ecole Normale Supérieure in Lyon (ENS Lyon). The NLTD glasses were leached using the protocol of Blichert-*Toft and Albarède* [2009], which uses hot 6 M HCl alternating between ultrasonication and heating for about an hour. The Rotuma and Fiji Island basaltic chips were leached following the procedures outlined in *Price et al*. [2016], which in addition to using hot 6 M HCl also uses hot 4 M HNO_3 and hot 30% H_2O_2.

Following leaching and rinsing, all samples were dissolved in a 3:1 mixture of concentrated double-distilled HF and HNO_3 followed by evaporation to dryness after digestion for 48 h at 130°C. Hafnium was separated from all the samples in this study by leaching the samples for 48 hours with concentrated double-distilled HF and then taking the HF supernatant containing the Hf through two successive anion-exchange and cation-exchange columns following the methods outlined in *Blichert-Toft et al*. [1997]. The CaMg-fluoride precipitates resulting from the HF leaching step, which contained the Pb, Sr, and Nd, were redissolved in 6 M HCl after first fuming them with double-distilled $HClO_4$ to decompose the fluorides.

Lead columns for the Rotuma and Fiji Island samples were run at ENS Lyon using microcolumns loaded with Biorad AG1-X8 resin. Strontium and Nd were recovered from the clean wash off the Pb columns using 1M HBr and transported to the University of North Carolina, Chapel Hill (UNC), while the Pb was eluted with 6M HCl and analyzed at ENS Lyon (see below). For the NLTD samples, the fraction hosting Sr, Nd, and Pb following dissolution and leaching out of the Hf at ENS Lyon was transported to Boston University (BU) where Pb was separated on Biorad AG1-X8 columns [following *Price et al*., 2014]; Sr and Nd for these samples also were recovered from the clean wash off the Pb columns using 0.7 M HBr, while Pb was eluted with 6 M HCl.

Strontium and Nd for the NLTD samples were separated using ion-exchange chromatography at BU: Sr was separated using Eichrom Sr-spec resin and Nd was separated using a two-step protocol involving Eichrom TRU resin followed by Eichrom LN-Spec resin (following methods in *Price et al*. [2014]). Strontium and Nd for the Fiji and Rotuma Island samples were separated at UNC. At UNC the samples were split and Sr separated from one portion using Eichrom Sr-spec, while Nd was separated from the other portion following a three-step protocol involving AGW50x-4 resin and HCl, Eichrom TRU resin, and AGW50x-4 resin with 2-methyl-lactic acid (MLA).

For all samples, Hf, Pb, Sr, and Nd were separated from the same sample dissolutions, thereby minimizing sample consumption and avoiding potential sample heterogeneity. The total procedural blanks for Hf, Pb, Sr, and Nd of the NLTD samples are $<$20 pg, $<$30 pg, $<$80 pg, and $<$35 pg, respectively [*Price et al*., 2014 and J. Blichert-Toft routine blank measurements], while the total procedural blanks for the Rotuma and Fiji samples are $<$20 pg, $<$20 pg, $<$100 pg, and $<$50 pg (J. Blichert-Toft routine blank measurements). The blanks are all negligible relative to the amount of sample Sr, Nd, Pb, and Hf analyzed.

Hafnium isotopic compositions for all samples (i.e., NLTD, Fiji and Rotuma samples) were determined by multicollector inductively coupled plasma mass spectrometry (MC-ICP-MS) on the Nu Plasma 500 HR at ENS Lyon. Lead, Sr, and Nd isotopic compositions for the NLTD samples likewise were measured by MC-ICP-MS on the Thermo-Finnigan Neptune at Woods Hole Oceanographic Institution (WHOI); the column chemistry and mass spectrometry for the NLTD samples were carried out during the same analytical sessions as the sample unknowns (and unleached USGS reference materials) analyzed in *Price et al*. [2014]. Lead isotopic compositions for the Fiji and Rotuma Island samples were analyzed on the Nu Plasma 500 HR at ENS Lyon while the Sr and Nd isotopic compositions of these samples were determined by thermal ionization mass spectrometry (TIMS) at UNC on the VG Sector 54 and Phoenix, respectively; the column chemistry and mass spectrometry for the Fiji and Rotuma samples were carried out during the same analytical sessions as the unleached USGS reference materials. The new radiogenic isotopic data for the basaltic unknowns and the USGS reference materials are provided in Table 1. Details on the measurement and standard normalization protocols are as follows:

3.3.1. Hafnium

For all samples, Hf isotopic measurements followed the protocol described by *Blichert-Toft et al*. [1997]. The JMC-475 Hf standard was analyzed every second sample and the unweighted mean $^{176}Hf/^{177}Hf$ ratios obtained during each day-long data collection session were 0.282166, 0.282170, 0.282170, 0.282171, 0.282172, 0.282172, 0.282163, 0.282170, and 0.282170. These values (the mean of which is 0.282169 ± 0.000007, 2SD, equivalent to an external reproducibility of 25 ppm (2σ)) are identical within error to the accepted value of 0.282163 ± 0.000009 [*Blichert-Toft et al*., 1997] for JMC-475, hence no corrections were applied to the data collected for this study. Although insignificant for all analyzed samples, the Hf isotopic ratios were corrected online for isobaric interferences of W and Ta on mass 180 and Lu and Yb on mass 176 by monitoring the interference-free isotopes ^{183}W, ^{181}Ta, ^{175}Lu, and ^{173}Yb, respectively. The data were corrected for instrumental mass fractionation relative to $^{179}Hf/^{177}Hf$ of 0.7325 using an exponential law.

3.3.2. Lead

At both WHOI and ENS Lyon, Pb isotopic compositions were measured by Tl addition (using a $^{205}Tl/^{203}Tl$ ratio of 2.38890) and sample-standard bracketing using the values for NIST SRM 981 of *Eisele et al*. [2003] ($^{206}Pb/^{204}Pb = 16.9409$, $^{207}Pb/^{204}Pb = 15.4976$, and $^{208}Pb/^{204}Pb = 36.7262$). The external reproducibility of the reported Pb isotope ratios measured at ENS Lyon as estimated from the repeated (every two samples) runs of NIST SRM 981 are 100–200 ppm (or 0.01–0.02%) for ratios containing 204 ($^{206}Pb/^{204}Pb$, $^{207}Pb/^{204}Pb$, $^{208}Pb/^{204}Pb$) and 50 ppm (or 0.005%) for $^{207}Pb/^{206}Pb$, $^{208}Pb/^{206}Pb$, and $^{207}Pb/^{208}Pb$, while the external reproducibility of runs of the NIST SRM 981 at WHOI is better than 117 ppm (2σ) for $^{206}Pb/^{204}Pb$, $^{207}Pb/^{204}Pb$, and $^{208}Pb/^{204}Pb$ [*Hart et al*., 2004].

3.3.3. Strontium

For samples measured by MC-ICP-MS, intensities were measured on masses 82–88 and corrections for isobaric interferences on masses 87 (Rb), 84 (Kr), and 86 (Kr) were made offline following the procedures outlined in *Jackson and Hart* [2006]. Isotopic ratios of Sr were corrected for instrumental mass bias relative to $^{86}Sr/^{88}Sr$ of 0.1194 using an exponential law. Measured $^{87}Sr/^{86}Sr$ ratios of the samples were corrected for the offset between the measured and preferred $^{87}Sr/^{86}Sr$ values (0.710240) [*Jackson and Hart*, 2006] for SRM 987. The external precision of the $^{87}Sr/^{86}Sr$ measurements is estimated to be 15–25 ppm (2σ) [*Hart and Blusztajn*, 2006].

For $^{87}Sr/^{86}Sr$ measurements by TIMS at UNC, methods are reported in *Hedman et al*. [2009]. Isotopic ratios of Sr were corrected for instrumental mass bias using an exponential law and an $^{86}Sr/^{88}Sr$ ratio of 0.1194. The $^{87}Sr/^{86}Sr$ ratios measured in the samples were normalized by the offset between the average measured value of SRM 987 during the analytical session (0.710256 ± 0.000013, 2SD) and the preferred $^{87}Sr/^{86}Sr$ of 0.710240 [*Jackson and Hart*, 2006]. The external precision of the $^{87}Sr/^{86}Sr$ measurements on the VG Sector 54 at UNC is estimated to be 20 ppm (2σ).

3.3.4. Neodymium

For samples measured by MC-ICP-MS on the Thermo-Finnigan Neptune at WHOI, Nd isotopic compositions were corrected for instrumental mass fractionation relative to $^{146}Nd/^{144}Nd$ of 0.7219 using an exponential law. The JNdi-1 and La Jolla Nd standards were run during each analytical session. The $^{143}Nd/^{144}Nd$ values for JNDi-1 were adapted to the La Jolla $^{143}Nd/^{144}Nd$ value using a conversion factor of 1.000503 [*Tanaka et al*., 2000]. When the preferred JNdi-1 value (0.512104) [*Jackson and Carlson*, 2012] is adapted to the La Jolla $^{143}Nd/^{144}Nd$ using a ratio of 1.000503 [*Tanaka et al*., 2000], the preferred La Jolla value is 0.511847. The La Jolla and La Jolla-renormalized JNdi-1 $^{143}Nd/^{144}Nd$ measurements were averaged to give a final La Jolla average for the analytical session; measured sample $^{143}Nd/^{144}Nd$ ratios were corrected for the offset between measured and preferred (0.511847) La Jolla $^{143}Nd/^{144}Nd$ values [*White and Patchett*, 1984]. The external precision of the $^{143}Nd/^{144}Nd$ measurements at WHOI is estimated to be 15–25 ppm (2σ) [*Hart and Blusztajn*, 2006].

For TIMS $^{143}Nd/^{144}Nd$ measurements at UNC, Nd was run as an oxide on the IsotopX Phoenix. Oxide corrections follow *Harvey and Baxter* [2009]. Neodymium isotopic compositions were corrected for instrumental mass fractionation relative to a $^{146}Nd/^{144}Nd$ value of 0.7219 using an exponential law. The standard JNdi-1 was run during the analytical session, and the average $^{143}Nd/^{144}Nd$ JNdi-1 value from the analytical session was 0.512103 ± 0.000012 (2SD [$n = 7$]). The $^{143}Nd/^{144}Nd$ ratios for unknowns were corrected for the offset between our average measured value of the JNdi-1 standard during the analytical session and the preferred JNdi-1 $^{143}Nd/^{144}Nd$ (0.512104). The external precision of the $^{143}Nd/^{144}Nd$ measurements on the UNC IsotopX Phoenix is estimated to be better than 20 ppm (2σ).

3.4. He Isotopic Analysis

Helium abundances and isotopic ratios from subaerial Fiji and Rotuma Island samples were measured on olivine phenocrysts at WHOI using an automated dual-collection, statically operated He isotope mass spectrometer. The measurements were all made by crushing olivines in vacuo, following the protocol of *Kurz et al*. [2004]. Helium gas concentrations (^4He) in the samples run at WHOI ranged from 2.08×10^{-9} to 1.97×10^{-8} cc STP/g, and internal precision of the $^3He/^4He$ measurements ranged from 0.25 to 0.54 Ra (2σ). $^3He/^4He$ ratios are reported relative to atmospheric (R/Ra) using an atmospheric $^3He/^4He$ ratio of 1.384×10^{-6}. The new $^3He/^4He$ data are presented in Table 2, and range from 6.7 to 8.1 Ra.

Table 2. He Isotopic Analyses on Rotuma and Fiji Island Lavas

Sample Location	Sample Name	Phase Analyzed	Sample Mass (g)	$^3He/^4He^a$	Error (2σ)[b]	^4He (cc STP/g)
Fiji lavas						
Fiji (Koro, Type I FOIB)	W251	Olivine	0.1054	7.16	0.37	8.28E-009
Fiji (Mago, Type I FOIB)	Mago	Olivine	0.1130	7.65	0.28	1.97E-008
Fiji (Taveuni, Type I FOIB)	WQ64	Olivine	0.2710	8.08	0.35	6.48E-009
Fiji (Taveuni, Type I FOIB)	FJ-12-5	Olivine	0.1507	7.88	0.54	2.08E-009
Fiji (Vatu-i-ra, Type I FOIB)	WQ208	Olivine	0.1998	6.73	0.39	2.46E-009
Fiji (Suvasuva, Type I/II FOIB)	WQ28	Olivine	0.1387	7.12	0.36	5.44E-009
Rotuma lavas						
Rotuma, Oinafa Basalt 2	ROT-3	Olivine	0.2703	7.78	0.25	1.26E-008
Rotuma, Oinafa Basalt 1	ROT-4	Olivine	0.2205	7.50	0.30	6.74E-009
Rotuma, Oinafa Basalt 2	ROT-12	Olivine	0.2464	7.14	0.29	6.25E-009

[a]All $^3He/^4He$ ratios are reported relative to the atmospheric ratio (R/Ra) of 1.384×10^{-6}.
[b]Error is 2σ standard error of the mean, and is absolute (not relative), and are for the last digits of the reported isotopic ratio. Errors represent internal (in-run) precision.

4. Results

4.1. Major and Trace Element Compositions

Major element compositions from the new Rotuma rocks show that, with one exception (sample ROT-11), they are all alkali lavas; ROT-11 falls in the tholeiitic field (supporting information Data Set 1 and Figure S1). Furthermore, all the Rotuma lavas are basaltic, with the exception of sample ROT-6, which falls in the trachy-basalt field (supporting information Figure 1). Primitive mantle normalized plots show that the Rotuma lavas are enriched in incompatible elements (supporting information Data Set 2 and Figure S2).

New major element compositions for Fijian ocean island basalts examined in this study are reported in supporting information Table 1. Additionally, supporting information Table 1 summarizes previously published major element data [*Gill and Whelan*, 1989; *Pearce et al*., 2007] for the samples that are characterized for radiogenic isotopes in this study. The major element data for Rotuma lavas and Fijian OIB are shown in supporting information Figure 2, together with previously published data. New and previously published major element data reveal that the Fijian lavas characterized in this paper fall in the fields of trachy-basalt (samples W271a and W135), alkali basalt (samples FJ-12-3, WQ7b, WQ208, Mago, W251, and WQ28), and tholeiite basalt (samples FJ-12-5 and WQ64) (supporting information Figure S1); major and some trace element data for samples W271a, W135, WQ7b, WQ208, and WQ28 are presented in *Gill and Whelan* [1989] and *Pearce et al*. [2007] (supporting information Data Sets 1 and 2). New trace element data of the subset of Fiji OIB lavas characterized for radiogenic isotopes in this study are also reported in supporting information Data Set 2. Primitive mantle normalized plots show that all of the Fijian samples examined in this study are enriched in the most incompatible elements. The lavas show strong depletions in Pb and most samples exhibit enrichment in Sr (supporting information Figure S2). Compared to published trace element data from Fijian OIB, the lavas presented here show similar, OIB-like primitive mantle normalized trace element patterns (supporting information Figure S2).

4.2. Hf-Pb-Sr-Nd-He Isotopic Compositions

Isotopic data for the new samples in this study are shown in Table 1. In the figures showing the new isotopic data (Figures 2 and 3) we also show (as individual data points) relevant data that were published previously, including data from the South Pandora Ridge, Fiji Triple Junction, Yasawa-Yadua Volcanic Zone, Rochambeau Bank and Rifts, and the Northeast Lau Basin (NELB). Additionally, we show data fields representing previously published data from Samoa (shield and rejuvenated lavas), Rurutu hot spot, Louisville hot spot, Rarotonga hot spot, Uo Mamae Seamount (which hosts a geochemically extreme EM1 composition in the region of Samoa and the Lau Basin), Niuafo'ou Island (which hosts an enriched mantle signature in the Lau Basin), the Tonga arc, Fijian arc lavas, the Foualei Rift and spreading center (FRSC) and the Central Lau Spreading Center (CLSC). We note that while Uo Mamae seamount defines a field distinct from that of the Rarotonga hot spot in Figures 2 and 3, *Price et al*. [2016] argue that they are genetically related and their geochemical signatures ultimately derived from the same hot spot: Uo Mamae and Rarotonga Island share common EM1 geochemical signatures (stronger in the former), and Uo Mamae seamount lies on the

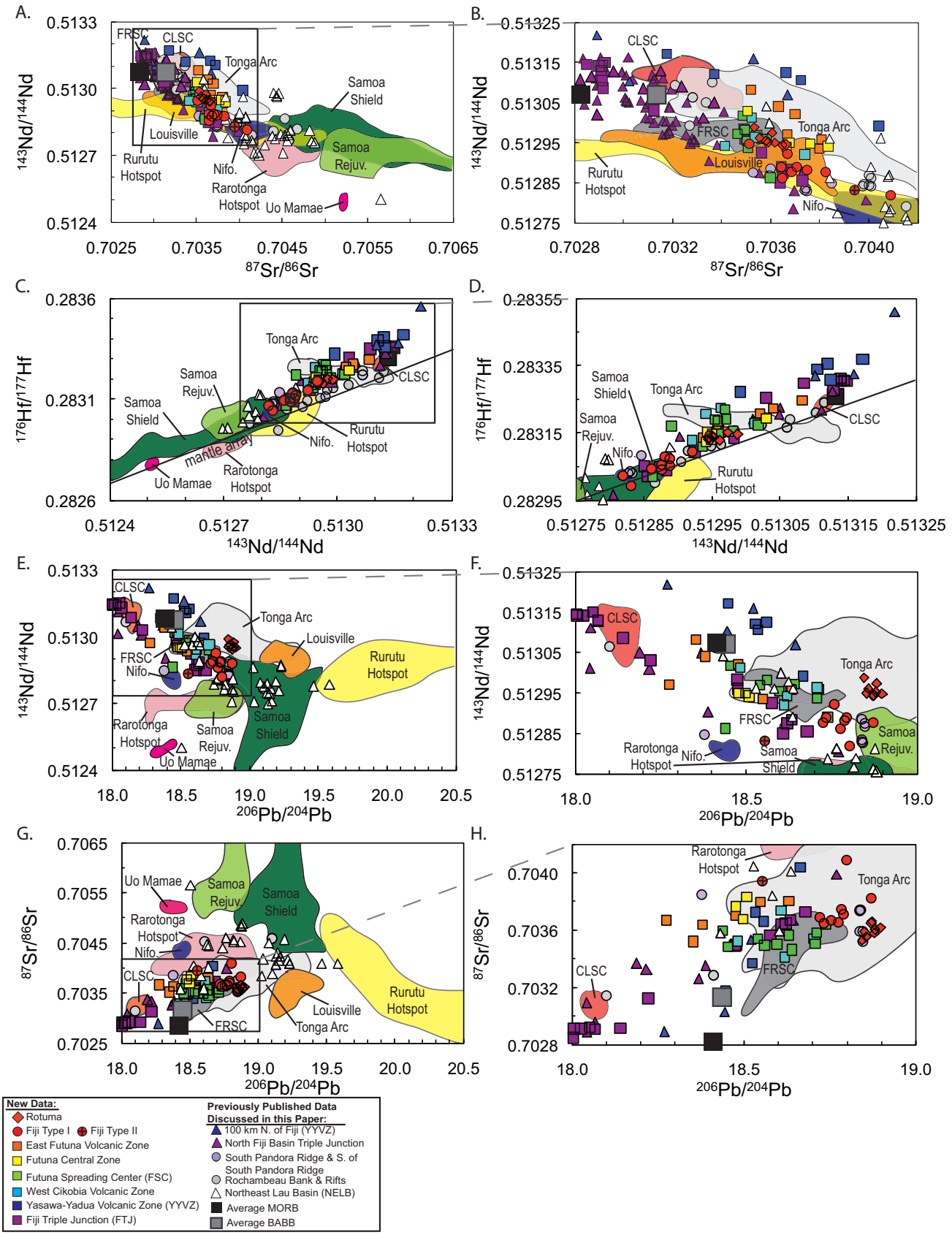
A.
B.
C.
D.
E.
F.
G.
H.
FRSC
CLSC
Tonga Arc
Samoa Shield
Louisville
Rurutu Hotspot
Samoa Rejuv.
Nifo.
Rarotonga Hotspot
Uo Mamae
mantle array
$^{87}Sr/^{86}Sr$
$^{143}Nd/^{144}Nd$
$^{176}Hf/^{177}Hf$
$^{206}Pb/^{204}Pb$
New Data:
Rotuma
Fiji Type I
Fiji Type II
East Futuna Volcanic Zone
Futuna Central Zone
Futuna Spreading Center (FSC)
West Cikobia Volcanic Zone
Yasawa-Yadua Volcanic Zone (YYVZ)
Fiji Triple Junction (FTJ)
Previously Published Data Discussed in this Paper:
100 km N. of Fiji (YYVZ)
North Fiji Basin Triple Junction
South Pandora Ridge & S. of South Pandora Ridge
Rochambeau Bank & Rifts
Northeast Lau Basin (NELB)
Average MORB
Average BABB

reconstructed hot spot track of the Rarotonga hot spot. The source of Uo Mamae lavas was influenced by prior passage of the lithosphere (beneah Uo Mamae) over the Rarotonga hot spot at ~15 Ma.

4.2.1. Fiji Triple Junction

The westernmost sample locality in this study, the Fiji Triple Junction, is located in the North Fiji Basin, ~ 375 km south of South Pandora Ridge and ~375 km west of the largest island of Fiji, Viti Levu (Figure 1). The 16 new lavas dredged from 12 locations near the Fiji Triple Junction form a broad array in all isotopic spaces that is anchored by a depleted, MORB-like sample (NLTD-45-2) at one end and a more enriched sample (NLTD-40-1) at the other end (Figures 2 and 3). The depleted end-member identified in this study (i.e., lowest $^{87}Sr/^{86}Sr$), sample NLTD-45-2, has $^{143}Nd/^{144}Nd$ of 0.513150, $^{87}Sr/^{86}Sr$ of 0.702908, $^{206}Pb/^{204}Pb$ of 18.0582, and $^{176}Hf/^{177}Hf$ of 0.283304; the enriched end-member sample (i.e., highest $^{87}Sr/^{86}Sr$), NLTD-40-1, has $^{143}Nd/^{144}Nd$ of 0.512855, $^{87}Sr/^{86}Sr$ of 0.703728, $^{206}Pb/^{204}Pb$ of 18.6846, and $^{176}Hf/^{177}Hf$ of 0.283023. This broad array overlaps with previous data on lavas from the North Fiji Basin, including the Fiji Triple Junction region [e.g. *Price et al*., 2014; shown as previously published data in Figures 1–3]. Notably, a lava with even more geochemically enriched radiogenic isotopic compositions has been found in the northern region of the Fiji Triple Junction region (sample 54-10-1 from segment N160 with $^{87}Sr/^{86}Sr$ and $^{143}Nd/^{144}Nd$ of 0.703985 and 0.512805, respectively, from *Nohara et al*. [1994]). In several radiogenic isotopic spaces (Figures 2 and 3), the most geochemically enriched Fiji Triple Junction lavas plot near, or inside, the field for geochemically enriched lavas from nearby South Pandora Ridge (see Figure 1) that were described in *Price et al*. [2014]. However, South Pandora Ridge is not a perfect compositional match for the enriched end-member identified at Fiji Triple Junction, as the enriched portion of the Fiji Triple Junction array is shifted slightly away from the enriched South Pandora Ridge component towards a more geochemically enriched component (e.g., with higher $^{87}Sr/^{86}Sr$, lower $^{143}Nd/^{144}Nd$, and lower $^{176}Hf/^{177}Hf$) that is similar to Samoan lavas. In fact, in several isotopic spaces (e.g., $^{143}Nd/^{144}Nd$ versus $^{176}Hf/^{177}Hf$ and $^{206}Pb/^{204}Pb$ versus $^{208}Pb/^{204}Pb$), the most enriched Fiji Triple Junction lavas overlap the fields for Samoan shield and rejuvenated lavas.

4.2.2. Yasawa-Yadua Volcanic Zone

The next dredge region to the East, the Yasawa-Yadua Volcanic Zone, is located ~400 km east of the Fiji Triple Junction and ~100 km north of the largest Island of Fiji, Viti Levu (Figure 1) (this sampling region was referred to as "100 km North of Viti Levu" in *Price et al*. [2014]). The five new samples from the four different dredges of the Yasawa-Yadua Volcanic Zone show a broad range of radiogenic isotopic compositions: when compared to the Fiji Triple Junction isotopic data and other isotopic data from the Lau and North Fiji Basin lavas, the Yasawa-Yadua Volcanic Zone data are shifted to higher $^{143}Nd/^{144}Nd$ at a given $^{206}Pb/^{204}Pb$, $^{207}Pb/^{204}Pb$, $^{208}Pb/^{204}Pb$, and $^{87}Sr/^{86}Sr$ (Figures 2 and 3). The Yasawa-Yadua Volcanic Zone array is anchored

Figure 2. Sr, Nd, Hf, and Pb isotopic relationships among new lavas dredged from the Lau and North Fiji Basins, Rotuma Island and Fijian Islands. The first (left) column of panels shows the new data in the context of all possible end-members in the region, while the close-up panels (right colum) highlight the new data presented here. The data are shown together with data fields for lavas from the Samoan hot spot track, Rurutu hot spot track, Rarotonga hot spot track (and Uo Mamae seamout), and Louisville hot spot track. In addition to the new data, previously published data from the South Pandora Ridge [*Price et al*., 2014], Fiji Triple Junction [*Nohara et al*., 1994; *Price et al*., 2014], Yasawa-Yadua Volcanic Zone (shown as 100 km N of Fiji in *Price et al*. [2014]), Rochambeau Bank and Rifts [*Lytle et al*., 2012; *Nebel and Arculus*, 2015] and the Northeast Lau Basin [*Falloon and Crawford*, 1991; *Danyushevsky et al*., 1995; *Falloon et al*., 2007, 2008; *Caulfield et al*., 2012, 2015; *Price et al*., 2016] are shown as symbols for reference. MORB is mid-ocean ridge basalt and BABB is back-arc basin basalt. The average MORB and average BABB data are from *Gale et al*. [2013], except for panels C and D (because sufficiently precise Hf isotopic data are not available). Data for the Central Lau Spreading Center (CLSC) field are from *Boespflug et al*. [1990], *Loock et al*. [1990], *Hergt and Woodhead* [2007], *Pearce et al*. [2007], and *Regelous et al*. [2008]. Rarotonga hot spot data, which include lavas from Rarotonga Island and Aitutaki Island, are from *Nakamura and Tatsumoto* [1988], *Hauri and Hart* [1993], *Salters and White* [1998], *Tatsumi et al*. [2000], *Schiano et al*. [2001], *Hanyu et al*. [2011], and *Salters et al*. [2011]. While we believe that Uo Mamae and the Rarotonga Hot spot are related, we plot them as separate fields but as similar colors. The Uo Mamae data are from *Pearce et al*. [2007] and *Regelous et al*. [2008]. Rurutu hot spot data, which include lavas from the young series of Arago Seamount, the young series of Rurutu Island, Mauke Island, and Atiu Island, are from *Nakamura and Tatsumoto* [1988], *Chauvel et al*. [1992, 1997], *Hauri and Hart* [1993], *Hemond et al*. [1994], *Woodhead* [1996], *Kogiso et al*. [1997], *Salters and White* [1998], *Schiano et al*. [2001], *Lassiter et al*. [2003], *Bonneville et al*. [2006], *Salters et al*. [2011], and *Hanyu et al*. [2011]. Rurutu sample 74-394 from *Chauvel et al*. [1997] is excluded from this field [*Chauvel et al*., 1997 ignored this sample due to its unusual geochemistry and we note that it is a cobble of unknown origin]. Values for Samoan data fields are from *Wright and White* [1987], *Poreda and Craig* [1992], *Workman et al*. [2004], *Workman and Hart* [2005], *Jackson et al*. [2007a,b,], and *Salters et al*. [2011]. Louisville data are from *Cheng et al*. [1987], *Beier et al*. [2011], and *Vanderkluysen et al*. [2014]. Louisville samples identified as highly altered or very highly altered were excluded. Niuafo'ou data are from *Regelous et al*. [2008] and *Tian et al*. [2011] and are shown as they represent geochemically extreme compositions from the Lau Basin. Fonualei Rift and Spreading Center (FRSC) data are from *Escrig et al*. [2012]. Tonga Arc data are from *Hergt and Woodhead* [2007], *Escrig et al*. [2012], *Turner et al*. [2012], and *Caulfield et al*. [2012, 2015]. Panels C and D include a line representing the mantle array from *Vervoort et al*. [1999] defined as $\varepsilon_{Hf} = 1.33^{*}\varepsilon_{Nd} + 3.19$, where the Nd and Hf epsilon notations were calculated using the CHUR values of $^{143}Nd/^{144}Nd = 0.512638$ [*Jacobsen and Wasserburg*, 1980 and *Hamilton et al*., 1983] and $^{176}Hf/^{177}Hf = 0.282772$ [*Blichert-Toft and Albarède*, 1997].

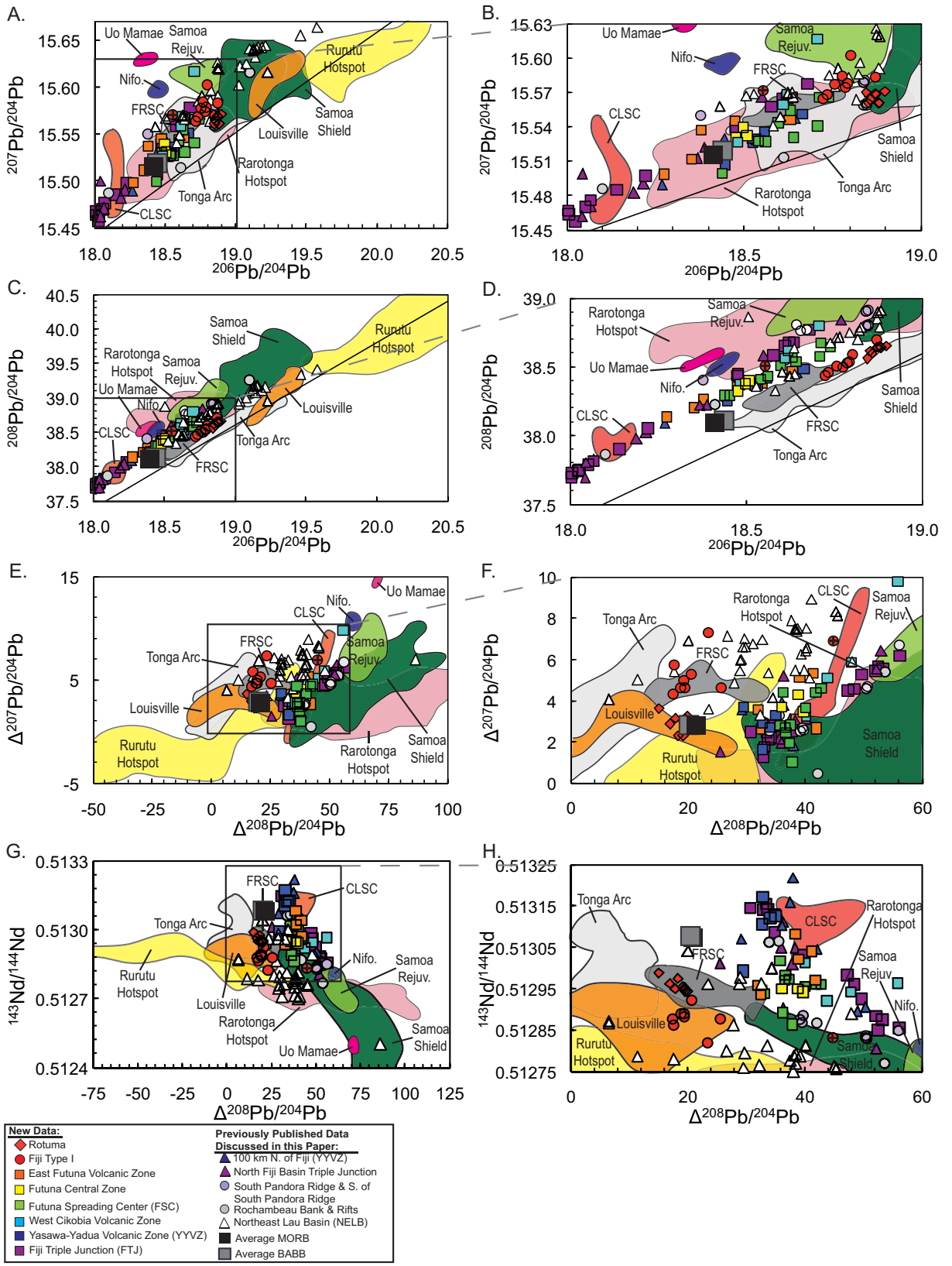

Figure 3. Sr, Nd, Hf, and Pb isotopic relationships among new lavas dredged from the Lau and North Fiji Basins. Data shown in the figures are as in Figure 3. The data and data fields are from references provided in Figure 2. (a–d) The Northern Hemisphere reference line (NHRL) from *Hart* [1984]. $\Delta^{207}Pb/^{204}Pb$ and $\Delta^{208}Pb/^{204}Pb$ are defined in by *Hart* [1984] in the following way: $\Delta^{207}Pb/^{204}Pb = 0.1084(^{207}Pb/^{204}Pb) + 13.491$, and $\Delta^{208}Pb/^{204}Pb = 1.209(^{208}Pb/^{204}Pb) + 15.627$.

by a depleted mantle (MORB-like) composition on one end (sample NLTD-4-2, with $^{143}Nd/^{144}Nd$ of 0.513172, $^{87}Sr/^{86}Sr$ of 0.703175, $^{206}Pb/^{204}Pb$ of 18.4516, and $^{176}Hf/^{177}Hf$ of 0.283370), while the more enriched end-member of the Yasawa-Yadua Volcanic Zone array, sample NLTD-3-6, displays $^{143}Nd/^{144}Nd$ of 0.512992, $^{87}Sr/^{86}Sr$ of 0.704024, $^{206}Pb/^{204}Pb$ of 18.6705, and $^{176}Hf/^{177}Hf$ of 0.283273. The Yasawa-Yadua Volcanic Zone array overlaps with previously published data on four lavas from this region (dredged 100 km North of Viti Levu; see *Price et al.* [2014] and Figures 1–3). However, compared to the Yasawa-Yadua Volcanic Zone data presented in *Price et al.* [2014], the new data extend to more geochemically enriched compositions and thus expand the compositional field of isotopic compositions identified in the Yasawa-Yadua Volcanic Zone region. Additionally, *Price et al.* [2014] identified a lava in the Yasawa-Yadua Volcanic Zone region, sample 162-1, that is more depleted than the new Yasawa-Yadua Volcanic Zone lavas reported here, and this sample has $^{143}Nd/^{144}Nd$ of 0.513218, $^{87}Sr/^{86}Sr$ of 0.702892, $^{206}Pb/^{204}Pb$ of 18.2692, and $^{176}Hf/^{177}Hf$ of 0.283510. To our knowledge, sample 162-1 has the most geochemically depleted $^{143}Nd/^{144}Nd$ and $^{176}Hf/^{177}Hf$ identified in the Lau or North Fiji Basin.

4.2.3. West Cikobia Volcanic Zone

The next dredge locality to the East, the West Cikobia Volcanic Zone, is located ~170 km northeast of the Yasawa-Yadua Volcanic Zone and ~120 km north of the Fijian island of Vanua Levu (Figure 1). We present new data for four new lavas from four different dredges. The West Cikobia Volcanic Zone lavas exhibit a relatively narrow range of radiogenic isotopic compositions. The lava with the most enriched Sr, Nd, and Hf isotopic compositions from West Cikobia, sample NLTD-7-12, has $^{143}Nd/^{144}Nd$ of 0.512921, $^{87}Sr/^{86}Sr$ of 0.703738, $^{206}Pb/^{204}Pb$ of 18.6159, and $^{176}Hf/^{177}Hf$ of 0.283129 (Figures 2 and 3). In contrast, the most depleted West Cikobia lava (i.e., lowest $^{87}Sr/^{86}Sr$), sample NLTD-35-3, has $^{143}Nd/^{144}Nd$ of 0.512941, $^{87}Sr/^{86}Sr$ of 0.703396, $^{206}Pb/^{204}Pb$ of 18.6267, and $^{176}Hf/^{177}Hf$ of 0.283207 (Figures 2 and 3). The data from four lavas analyzed from the West Cikobia Volcanic Zone do not generally form clear arrays in multi-isotopic space (Figures 2 and 3). One exception is Pb isotopic space, which does show a well-defined array: sample NLTD-9-1 is significantly more radiogenic ($^{206}Pb/^{204}Pb$ of 18.7070, $^{207}Pb/^{204}Pb$ of 15.6167, and $^{208}Pb/^{204}Pb$ of 38.8015) than the lava from West Cikobia (sample NLTD-8-1) with the least radiogenic Pb ($^{206}Pb/^{204}Pb$ of 18.4872, $^{207}Pb/^{204}Pb$ of 15.5363, and $^{208}Pb/^{204}Pb$ of 38.4172). The radiogenic Pb isotopic composition in sample NLTD-9-1 tends to plot near lavas sampling enriched mantle compositions such as those sampled by Samoan rejuvenated lavas and lavas from Uo Mamae (Figure 3).

4.2.4. Futuna Spreading Center

The Futuna Spreading Center is located ~220 km east of West Cikobia and ~90 km west of Futuna Island. Geochemical data for 11 lavas from 10 different dredge locations, spanning ~125 km of the N-S trending Futuna Spreading Center, are reported here (Figure 1 and Table 1). The Futuna Spreading Center sample with the most geochemically enriched $^{87}Sr/^{86}Sr$ (NLTD-31-11, which exhibits $^{143}Nd/^{144}Nd$ of 0.512891, $^{87}Sr/^{86}Sr$ of 0.703625, $^{206}Pb/^{204}Pb$ of 18.7438, and $^{176}Hf/^{177}Hf$ of 0.283170) is shifted only slightly in isotopic space from the sample with the most geochemically depleted $^{87}Sr/^{86}Sr$ (NLTD-30-24 with $^{87}Sr/^{86}Sr$ of 0.703443, and $^{176}Hf/^{177}Hf$ of 0.283160) (Figures 2 and 3). One sample from the Futuna Spreading Center (NLTD-28-20) plots away from the main cluster of Futuna Spreading Center data in several isotopic spaces (e.g., $^{143}Nd/^{144}Nd$ versus $^{87}Sr/^{86}Sr$, $^{143}Nd/^{144}Nd$ versus $^{206}Pb/^{204}Pb$), and this lava has the lowest $^{143}Nd/^{144}Nd$ (0.512862) and the least radiogenic Pb isotopic ratios ($^{206}Pb/^{204}Pb$ of 18.4382, $^{207}Pb/^{204}Pb$ of 15.4999, $^{208}Pb/^{204}Pb$ of 38.2966) at this spreading center.

4.2.5. Futuna Central Zone

Lavas from the Futuna Central Zone are located ~125 km east of the Futuna Spreading Center and ~70 km south-southeast of Futuna Island. We present data for five new lavas from five different dredges. The lavas from this locality cluster together in radiogenic isotopic spaces: the most geochemically enriched sample from the Futuna Central Zone (NLTD-26-7) has $^{87}Sr/^{86}Sr$ of 0.703826, $^{143}Nd/^{144}Nd$ of 0.512943, $^{176}Hf/^{177}Hf$ of 0.283154, $^{206}Pb/^{204}Pb$ of 18.5147, $^{207}Pb/^{204}Pb$ of 15.5404, and $^{208}Pb/^{204}Pb$ of 38.4280; the most geochemically depleted lava (NLTD-23-12) has $^{87}Sr/^{86}Sr$ of 0.703489, $^{143}Nd/^{144}Nd$ of 0.513030, and $^{176}Hf/^{177}Hf$ of 0.283194 (note that Pb isotopic ratios are not available for this lava; Figures 2 and 3).

4.2.6. East Futuna Volcanic Zone

East Futuna Volcanic Zone lavas represent the easternmost samples, and thus the samples closest to the Samoan plume, presented in this study. The East Futuna Volcanic Zone is located ~70 km east of the Futuna Central Zone and ~80 km west of Rochambeau Bank and Rifts. We present geochemical data for six new lavas from seven different dredges. Much of the range in radiogenic isotopic compositions from the Futuna Volcanic Zone is captured by two samples: The most geochemically enriched (i.e., highest $^{87}Sr/^{86}Sr$) East

Futuna Volcanic Zone sample (NLTD-19-16 with $^{143}Nd/^{144}Nd$ of 0.512959, $^{87}Sr/^{86}Sr$ of 0.703805, $^{206}Pb/^{204}Pb$ of 18.6365, and $^{176}Hf/^{177}Hf$ of 0.283169) exhibits a moderate shift away from the most geochemically depleted (i.e., lowest $^{87}Sr/^{86}Sr$) East Futuna Volcanic Zone sample (NLTD-21-1 with $^{143}Nd/^{144}Nd$ of 0.513083, $^{87}Sr/^{86}Sr$ of 0.703518, $^{206}Pb/^{204}Pb$ of 18.3585, and $^{176}Hf/^{177}Hf$ of 0.283248) (Figures 2 and 3). However, sample NLTD-15-1 plots away from the other East Futuna Volcanic Zone samples, particularly in $^{143}Nd/^{144}Nd$ versus $^{206}Pb/^{204}Pb$ and $^{143}Nd/^{144}Nd$ versus $\Delta^{208}Pb/^{204}Pb$ isotopic spaces; this lava also has the least radiogenic Pb isotopic ratios ($^{206}Pb/^{204}Pb$ of 18.2742, $^{207}Pb/^{204}Pb$ of 18.4987, $^{208}Pb/^{204}Pb$ of 38.1384) of all East Futuna Volcanic Zone samples. Finally, while the East Futuna Volcanic Zone data partially overlap with the field defined by Futuna Spreading Center data in many radiogenic isotopic spaces, the East Futuna Volcanic Zone samples are shifted to higher $^{87}Sr/^{86}Sr$ at a given $^{143}Nd/^{144}Nd$ or $^{206}Pb/^{204}Pb$ (Figures 2 and 3).

4.2.7. Fijian Islands

A subset of the 10 subaerial, postarc Fijian island OIB lavas show the most geochemically enriched Sr, Nd, and Hf isotopic signatures and the most radiogenic Pb among the new data reported in this study (Figures 2 and 3). Eight of the 10 lavas sampled here fall within the Type I FOIB, as designated by *Gill and Whelan* [1989], because they show more geochemically depleted $^{87}Sr/^{86}Sr$ (i.e., $^{87}Sr/^{86}Sr < 0.703807$). We also present new data on one Type II FOIB (sample WQ7b), which has more geochemically enriched $^{87}Sr/^{86}Sr$ than the type I FOIB [*Gill and Whelan*, 1989]. An addition FOIB lava (sample WQ28) has geochemical characteristics similar to both Type I and Type II FOIB.

The most geochemically depleted lava from the Fijian lava group, sample W135, is a Type I FOIB from Talviuni Island. This lava has $^{143}Nd/^{144}Nd$ of 0.512946, $^{87}Sr/^{86}Sr$ of 0.703496, and $^{176}Hf/^{177}Hf$ of 0.283142; it does not have Pb isotopic data, but the eight Type I lavas presented here have relatively radiogenic $^{206}Pb/^{204}Pb$, extending up to 18.8700. The single Type II FOIB in this study, sample WQ7b, shows more geochemically enriched $^{87}Sr/^{86}Sr$ (0.703926), $^{143}Nd/^{144}Nd$ (0.512831), and $^{176}Hf/^{177}Hf$ (0.282994) and the least radiogenic $^{206}Pb/^{204}Pb$ (18.5540) of all the FOIB samples. In general, we note that the eight Type I FOIB have higher $^{143}Nd/^{144}Nd$, $^{176}Hf/^{177}Hf$ and $^{206}Pb/^{204}Pb$, and lower $^{87}Sr/^{86}Sr$, than Type II FOIB.

However, one FOIB lava (sample WQ28 from Suvasuva) is one of the most geochemically enriched lavas analyzed in this study and is neither clearly Type I nor Type II. This sample has the most geochemically enriched $^{143}Nd/^{144}Nd$ (0.512819), $^{87}Sr/^{86}Sr$ (0.704071) and $^{176}Hf/^{177}Hf$ (0.283022) of this study, isotopic signatures characteristic of Type II FOIB. However, it has less radiogenic $^{206}Pb/^{204}Pb$ (18.8022), more typical of Type I FOIB.

The most geochemically enriched Fijian lava reported previously has $^{87}Sr/^{86}Sr$ of 0.704082 (sample WQ28 from Seatura, *Pearce et al*. [2007]), which is similar to the most enriched $^{87}Sr/^{86}Sr$ reported here (sample WQ28 with $^{87}Sr/^{86}Sr$ of 0.704071). It is worth noting that one previously published $^{87}Sr/^{86}Sr$ value was much higher (0.70608, for sample WYK1; *Gill and Whelan* [1989]), but this sample, which had a high carbonate content, was not leached prior to analysis. Thus, the $^{87}Sr/^{86}Sr$ may not be a primary magmatic signature. Previous studies have also reported Fijian OIB samples with more geochemically depleted $^{87}Sr/^{86}Sr$ (0.70332 for sample 450 from Yanuyanu Island, *Gill and Whelan* [1989]) than reported for the lavas in this study. Previously reported $^{143}Nd/^{144}Nd$ and $^{176}Hf/^{177}Hf$ values in FOIB range from 0.512840 to 0.512880 [*Gill*, 1984; *Pearce et al*., 2007] and 0.282998 to 0.283007 [*Pearce et al*., 2007]. The $^{143}Nd/^{144}Nd$ and $^{176}Hf/^{177}Hf$ from our new data set range from 0.512819 to 0.512946 and 0.282994 to 0.283142, respectively, and thus extend the range of $^{143}Nd/^{144}Nd$ and $^{176}Hf/^{177}Hf$ for Fijian OIBs to both more geochemically enriched and depleted compositions. Previously reported $^{206}Pb/^{204}Pb$ from Fijian OIB ranged from 18.55 to 18.83 [*Gill*, 1984]. Thus, our new data set (which has $^{206}Pb/^{204}Pb$ that ranges from 18.5540 to 18.8700), extend the known range of $^{206}Pb/^{204}Pb$ in Fijian OIB to higher values.

We note that in $\Delta^{207}Pb/^{204}Pb$ versus $\Delta^{208}Pb/^{204}Pb$ isotopic space, two of the Fijian lavas overlap with the field for Fijian arc lavas. The remaining Fijian lavas overlap with the field for Fonualei Rift and Spreading Center, suggested by others [e.g., *Escrig et al*., 2012] to host a Tonga arc component. However, because the FOIB do not overlap with Fiji or Tonga arc lavas in other isotopic spaces, and the Fijian lavas do not exhibit trace element signatures associated with arc lavas (supporting information Table 2 and Figure 2), a clear arc signature is not suggested by the data.

The $^{3}He/^{4}He$ of lavas from the Fijian Islands (Table 2 and Figure 4) is the first reported for OIB from these Islands. All $^{3}He/^{4}He$ ratios fall in a range of 6.7–8.1 Ra, i.e., within the range for normal upper mantle values, as defined by MORB glass measurements [*Graham*, 2002; *Georgen et al*., 2003].

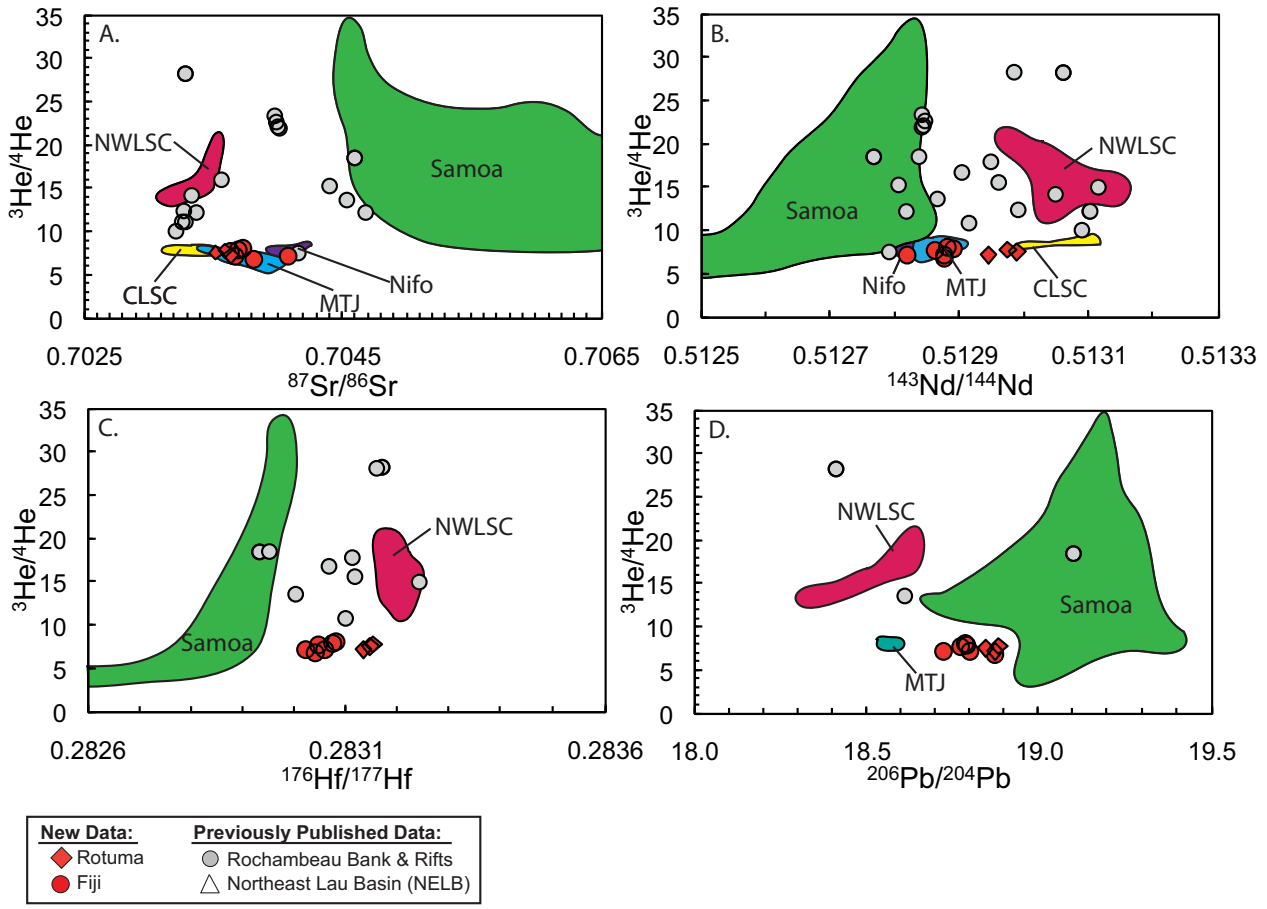

Figure 4. Helium isotopic data for lavas in this study plotted against their respective Pb-Sr-Nd-Hf isotopic ratios. Lavas from Rotuma and the Fijian Islands presented in this study show fairly limited variation in He-Pb-Sr-Nd-Hf isotopic ratios. Abbreviations: NWLSC *Northwest Lau Spreading Center*; MTJ *Mangatolu Triple Junction*; CLSC *Central Lau Spreading Center*, Nifo *Niuafo'ou*. Samoan data are from *Farley et al.* [1992], *Workman et al.* [2004], *Jackson et al.* [2007a,b]. Rochambeau Bank and Rifts data are from: *Volpe et al.* [1988], *Poreda and Craig* [1992], *Lupton et al.* [2009], *Tian et al.* [2011], *Hahm et al.* [2012], and *Lytle et al.* [2012]. The remaining data, all from locations in the Lau and North Fiji Basins, are from: *Hilton et al.* [1993], *Honda et al.* [1993], *Regelous et al.* [2008]; *Tian et al.* [2008, 2011], *Hahm et al.* [2012], *Lupton et al.* [2009], *Lytle et al.* [2012], *Price et al.* [2014, 2016], and *Nebel and Arculus* [2015]. The new data from Fiji and Rotuma (red symbols) do not show a high $^{3}He/^{4}He$ Samoan influence.

4.2.8. Rotuma Island

The Rotuma Island lavas tend to cluster together in radiogenic isotopic space: ROT-4 is the most geochemically depleted sample with $^{143}Nd/^{144}Nd$ of 0.512988, $^{87}Sr/^{86}Sr$ of 0.703517, $^{176}Hf/^{177}Hf$ of 0.283147 and $^{206}Pb/^{204}Pb$ of 18.8449; ROT-11 is the most geochemically enriched lava with $^{143}Nd/^{144}Nd$ of 0.512946, $^{87}Sr/^{86}Sr$ of 0.703646, $^{176}Hf/^{177}Hf$ of 0.283134, and $^{206}Pb/^{204}Pb$ of 18.8739 (Figures 2 and 3). These data greatly expand the available data for Rotuma lavas: only one previously published $^{87}Sr/^{86}Sr$ value exists for lavas from this island, and it is somewhat more radiogenic (0.70374; *Price and Kroenke* [1991]) than the highest $^{87}Sr/^{86}Sr$ reported here.

In general, the Rotuma lavas plot close to the Type I FOIB lavas in radiogenic isotopic spaces. However, the Rotuma lavas tend to be shifted toward more radiogenic $^{206}Pb/^{204}Pb$ and $^{208}Pb/^{204}Pb$, but less radiogenic $^{207}Pb/^{204}Pb$, than Type I FOIB. Additionally, Rotuma lavas tend to have slightly higher $^{143}Nd/^{144}Nd$ and $^{176}Hf/^{177}Hf$, and lower $^{87}Sr/^{86}Sr$, than Type I FOIB.

New $^{3}He/^{4}He$ data are presented for three of the Rotuma lavas and, similar to Fijian lavas, show a MORB-like range of 7.1–7.8 Ra (Table 2 and Figure 4). These represent the first $^{3}He/^{4}He$ analyses from Rotuma.

4.3. Geographic Variability Across Multiple Isotopic Systems

The compositions of new and previously published isotopic data on lavas from the Lau and North Fiji Basins are superimposed on a map of the region (Figures 5–7), revealing geographic patterns in the distribution of

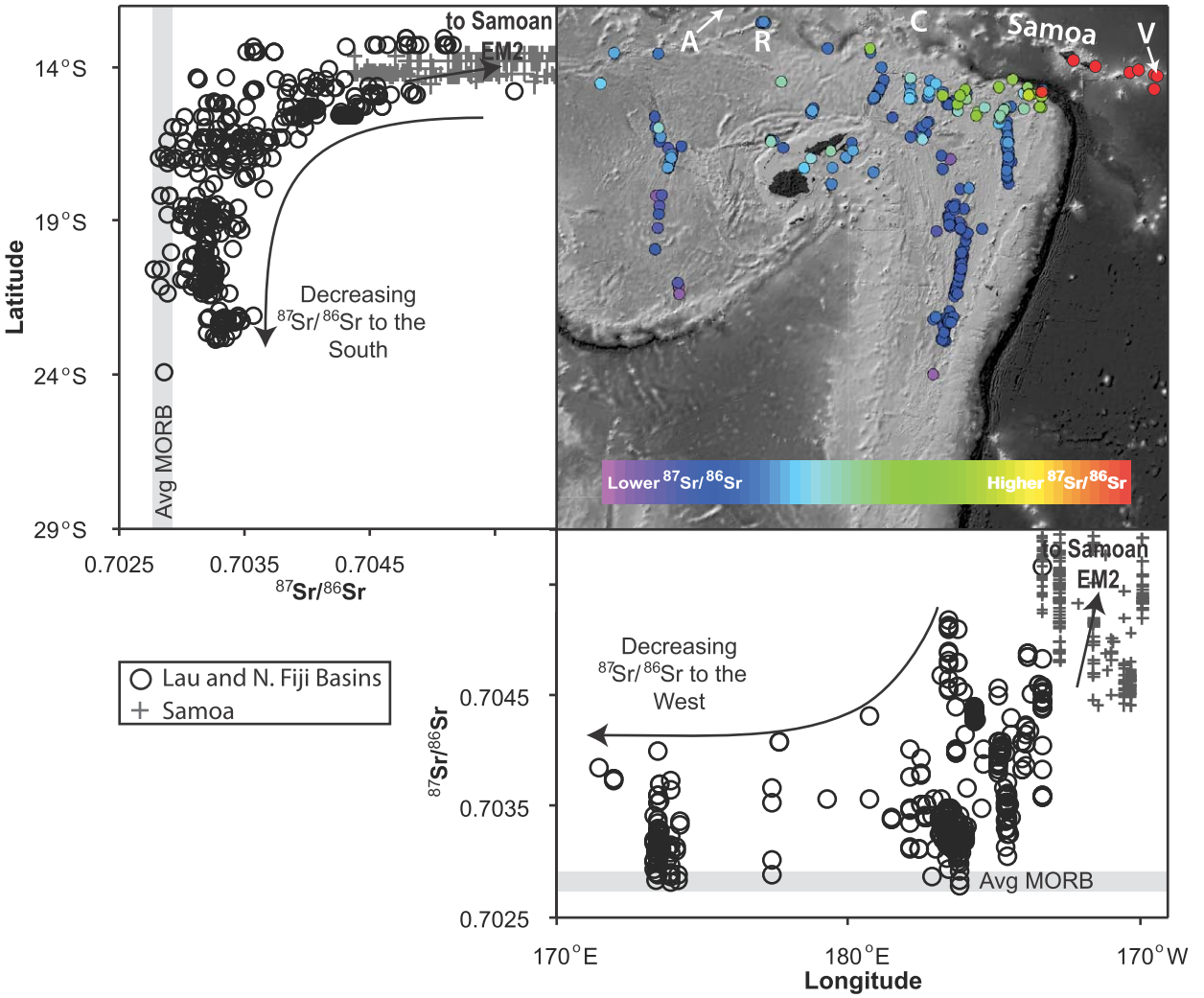

Figure 5. Map showing the distribution of new and previously published $^{87}Sr/^{86}Sr$ for lavas from the Lau and North Fiji Basins. Data on arc lavas are excluded, but data from young (<3 Ma) Fijian OIB are included. V is Vailulu'u, C is Combe Bank, R is Rotuma Island, and A is Alexa Bank. The color scale for $^{87}Sr/^{86}Sr$ ranges from blue (at low $^{87}Sr/^{86}Sr$) to red (at high $^{87}Sr/^{86}Sr$), but saturates at 0.705. We also include Samoan Sr isotopic data for reference. The $^{87}Sr/^{86}Sr$ data from Lau and North Fiji Basin lavas show a decrease to both the south and west, further from the location of the Samoan plume. Strontium isotopic data from the Lau and North Fiji Basins are from: *Boespflug et al.* [1990], *Danyushevsky et al.* [1995], *Escrig et al.* [2009, 2012], *Falloon et al.* [2007, 2008], *Falloon and Crawford* [1991], *Fretzdorff et al.* [2006], *Haase et al.* [2002, 2009], *Hergt and Woodhead* [2007], *Jackson et al.* [2010], *Loock et al.* [1990], *Lytle et al.* [2012], *Nohara et al.* [1994], *Poreda and Craig* [1992], *Price et al.* [2014, 2016], *Regelous et al.* [2008], *Tian et al.* [2008, 2011], and *Volpe et al.* [1988]. Samoan data are from: *Farley et al.* [1992], *Hauri et al.* [1993], *Jackson et al.* [2006, 2007, 2009, 2010, 2014], *Matsuda et al.* [1984], *Hofmann and White* [1982], *Workman et al.* [2004], and *Wright and White* [1987]. $^{87}Sr/^{86}Sr$ [*Gale et al.*, 2013] averages for MORB are from the literature.

isotopic signatures. Figure 5 shows the distribution of new and previously published $^{87}Sr/^{86}Sr$ data across the Lau and North Fiji Basins. The highest $^{87}Sr/^{86}Sr$ signatures are found in the northeast Lau Basin, only ~300 km east of where lavas with the highest $^{3}He/^{4}He$ (up to 28.1 Ra)—associated with incursion of a Samoan plume component—have been identified at Rochambeau Rifts [*Lupton et al.*, 2009] (Figures 5 and 6). The $^{87}Sr/^{86}Sr$ of lavas from the Lau and North Fiji Basins show both zonal and meridional gradients: the $^{87}Sr/^{86}Sr$ ratios decrease away from the northeast Lau Basin, toward the south and west (Figure 5). Similarly, $^{3}He/^{4}He$ exhibit maximum values in the northeast Lau Basin, and lower maximum values are observed to the south and west (Figure 6), including the new OIB-type lavas from Fiji and Rotuma Islands.

While broad gradients in a single isotopic system, $^{87}Sr/^{86}Sr$, illustrate the geographic trends in the geochemistry of Lau and North Fiji Basin lavas, evaluating the geographic variability of multiple isotopic systems can reveal different sources contributing to the geochemical makeup of the region (Figure 7). Figure 7a shows the covariation between $^{87}Sr/^{86}Sr$ (where the highest, most geochemically enriched $^{87}Sr/^{86}Sr$ ratios are

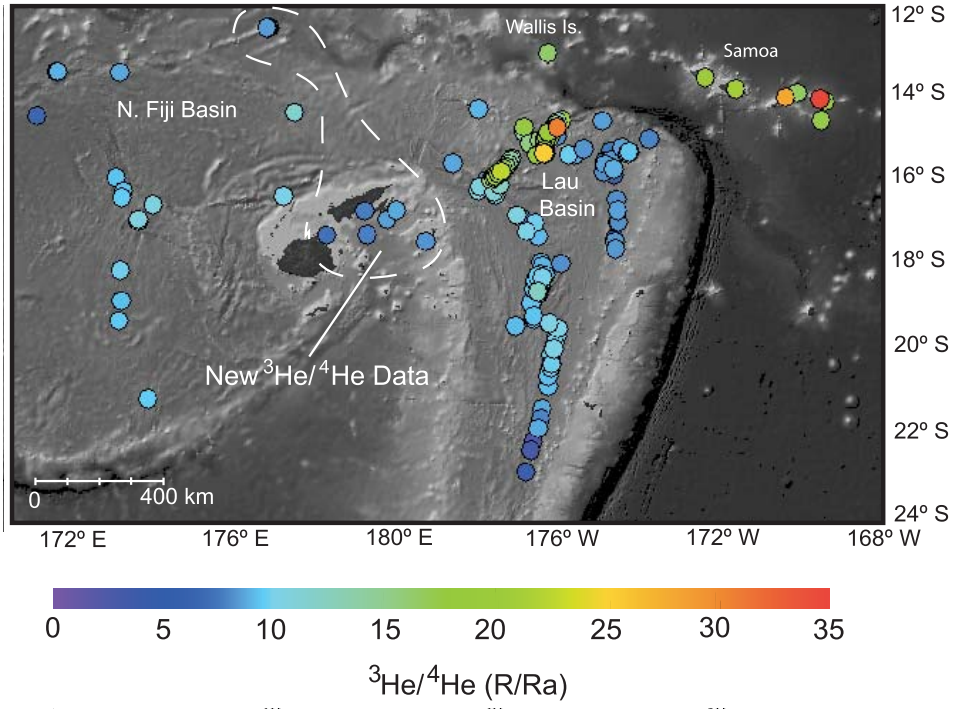

Figure 6. Map of the Lau and North Fiji Basins showing distribution of new and previously published ^{3}He/^{4}He. Also included are data from Samoa (only the highest ^{3}He/^{4}He found on each Samoan island is shown). The highest ^{3}He/^{4}He data are found in Rochambeau Bank lavas from the northern Lau Basin, and progressively lower ^{3}He/^{4}He ratios are found in lavas to the south and west of this region. Previously published isotopic data from the Lau and North Fiji Basins are from *Poreda and Craig* [1992], *Hilton et al.* [1993], *Honda et al.* [1993], *Nishio et al.* [1998], *Workman et al.* [2004], *Jackson et al.* [2007a,b], *Lupton et al.* [2009], *Hahm et al.* [2012], *Lupton et al.* [2015], and *Price et al.* [2014]. Base maps were created using GeoMapApp (http://www.geomapapp.org) with topographic and bathymetric data from SRTM_PLUS [*Becker et al.*, 2009].

represented by increasing symbol size in the map) and ^{143}Nd/^{144}Nd (where the lowest, most geochemically enriched ^{143}Nd/^{144}Nd ratios are represented with warmer colors) in lavas in the Lau and North Fiji Basins. The most salient observation is that the most geochemically enriched lavas (i.e., with the highest ^{87}Sr/^{86}Sr and lowest ^{143}Nd/^{144}Nd) are concentrated in the northeastern Lau Basin. Moving to the south and west, there is a gradual decrease in ^{87}Sr/^{86}Sr (shift to smaller symbols) and increase in ^{143}Nd/^{144}Nd (shift to cooler colors) as the lavas sample progressively more geochemically depleted mantle. Figure 7b shows how ^{87}Sr/^{86}Sr (variable color) and ^{206}Pb/^{204}Pb (variable size) covary as a function of geography in the region: lavas with the most geochemically enriched ^{87}Sr/^{86}Sr (warmest colors) and the most radiogenic ^{206}Pb/^{204}Pb (largest symbols) are found in the northeast Lau Basin. Figure 7c shows the correlation between ^{143}Nd/^{144}Nd (color variable) and ^{176}Hf/^{177}Hf (size variable) in lavas from the Lau and North Fiji Basins. Lavas with the most geochemically enriched ^{143}Nd/^{144}Nd (coolest color) and ^{176}Hf/^{177}Hf (largest size) tend to be found in the northeastern Lau Basin, while lavas with moderately enriched ^{143}Nd/^{144}Nd and ^{176}Hf/^{177}Hf can be found in Fiji and along the northern reaches of the Lau and North Fiji Basins. In summary, lavas from the northeastern Lau Basin, located closest to the Samoan hot spot, host the most geochemically enriched ^{87}Sr/^{86}Sr, ^{143}Nd/^{144}Nd, and ^{176}Hf/^{177}Hf and the most radiogenic Pb isotopic compositions in all of the Lau and North Fiji Basins.

5. Discussion

The first salient observation in the present study is that of clear gradients in ^{87}Sr/^{86}Sr, both meridional and zonal, across the northern Lau and North Fiji back-arc basins. The highest ^{87}Sr/^{86}Sr signatures are observed in the northeast Lau Basin, and these enriched signatures are absent in lavas to the south and west. A primary goal of the discussion below is to illuminate the processes responsible for generating these geochemical patterns in ^{87}Sr/^{86}Sr across the Lau and North Fiji Basins.

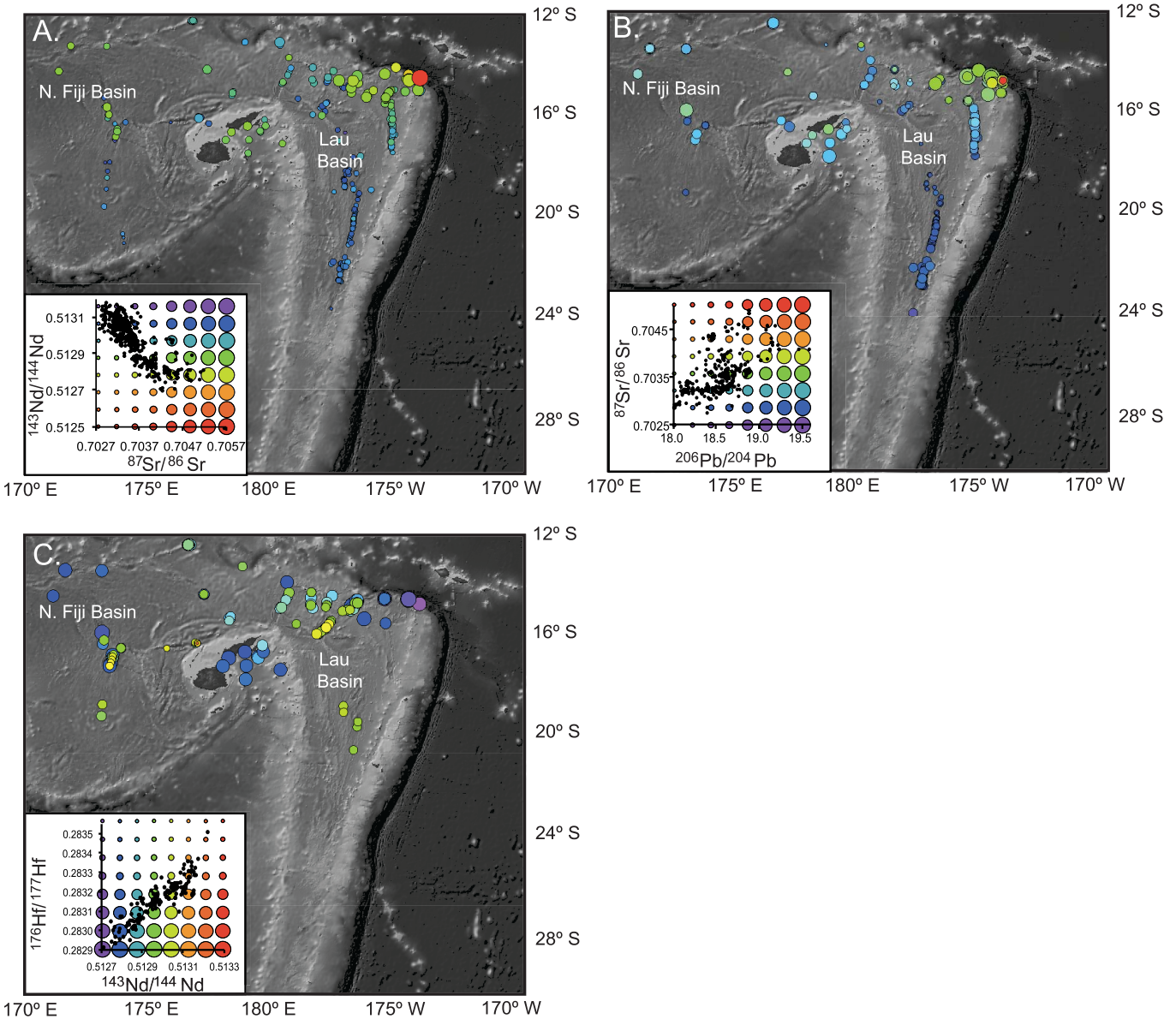

Figure 7. Maps of the Lau and North Fiji Basins showing the relationships between Hf, Pb, Sr, and Nd isotopic data of new and previously published samples. (a) The relationship between $^{87}Sr/^{86}Sr$ (size) and $^{143}Nd/^{144}Nd$ (color) as a function of geographic location for lavas in the Lau and North Fiji Basins, and (b) the relationship between $^{206}Pb/^{204}Pb$ (size) and $^{87}Sr/^{86}Sr$ (color) in the same lavas. (c) The relationship between $^{143}Nd/^{144}Nd$ (color) and $^{176}Hf/^{177}Hf$ (size). Arc data are not shown. Generally, lavas from the northeastern Lau Basin show the most geochemically enriched $^{87}Sr/^{86}Sr$, $^{143}Nd/^{144}Nd$, and $^{176}Hf/^{177}Hf$ and the most radiogenic Pb isotopic compositions of all lavas from the Lau and North Fiji Basins. The data used in these panels are from: *Boespflug et al.* [1990], *Danyushevsky et al.* [1995], *Escrig et al.* [2009, 2012], *Falloon et al.* [2007, 2008], *Falloon and Crawford* [1991], *Fretzdorff et al.* [2006], *Haase et al.* [2002, 2009], *Hergt and Woodhead* [2007], *Jackson et al.* [2010], *Jenner et al.* [1987], *Loock et al.* [1990], *Lytle et al.* [2012], *Nebel and Arculus* [2015], *Nohara et al.* [1994], *Pearce et al.* [2007], *Peate et al.* [1997], *Poreda and Craig* [1992], *Price et al.* [2014, 2016], *Regelous et al.* [2008], *Tian et al.* [2008, 2011], and *Volpe et al.* [1988].

Previous studies have established that geochemical components from the Samoan hot spot are present in lavas erupted in the northern Lau Basin [e.g., *Volpe et al.*, 1988; *Gill, and Whelan*, 1989; *Poreda and Craig*, 1992; *Wendt et al.*, 1997; *Ewart et al.*, 1998; *Pearce et al.*, 2007; *Tian et al.*, 2008, 2011; *Lupton et al.*, 2009; *Hahm et al.*, 2012; *Jenner at al.*, 2012; *Lytle et al.*, 2012; *Price et al.*, 2014, 2016; *Nebel and Arculus*, 2015]. Using Sr-Nd-Pb-Hf isotopic compositions, *Price et al.* [2014] argued that a component of Samoan mantle material exists in the North Fiji Basin far (up to 1400 km) to the west of the Samoan hot spot. Further work has established that, in addition to the influx of a Samoan component into the region, subduction of the older portions of the Rurutu and Rarotonga hot spots into the Tonga Trench has influenced the geochemistry of lavas in the northern Lau Basin [*Price et al.*, 2016]. Here using new and previously published geochemical

data, together with a plate reconstruction model for the region, we provide a conceptual geodynamic framework that accounts for the $^{87}Sr/^{86}Sr$ geochemical patterns across the northern Lau and North Fiji Basins.

5.1. Formation of East-West Geochemical Gradients in the Lau and North Fiji Basins

Based on plate reconstruction models, *Hart et al*. [2004] suggested that the Vitiaz Lineament—which separates the Lau and North Fiji Basins from the Pacific plate to the north—is the result of tearing of the Pacific plate along the northern terminus of the Tonga Trench. The locus of tearing has migrated eastward as the Tonga Trench approaches the Samoan hot spot, generating an East-West striking bathymetric low (Figures 1 and 8). At 4 Ma, *Hart et al*. [2004] place the northern terminus of the trench just to the south of Rotuma Island. Owing to rollback of the Pacific slab, the northern terminus of the Tonga Trench migrated ~500 km eastward (relative to the stationary Samoan plume) from 4 to 2 Ma, and was located just to the south of Combe Bank by 2 Ma [*Hart et al*., 2004] (Figure 8). Due to continued eastern migration of the northern terminus of the Tonga Trench over the past 2 Ma, the northern terminus migrated an additional ~500 km eastward, and is now located just ~150 km south of the Samoan island of Savai'i (and 400 km east-southeast of the volcanically active portion of the Samoan hot spot) [*Hart et al*., 2004] (Figure 8).

As the northern terminus of the Tonga Trench has approached the Samoan plume from the west over the past 4 Ma, the tearing Pacific plate has "unzipped" along a path that parallels, but is shifted ~100–200 km to the south of, the reconstructed trace of the Samoan hot spot track (Figures 1 and 8). This raises the possibility that relic Samoan plume material, attached to the base of the Pacific lithosphere, may have been continuously entrained by toroidal flow around the slab edge (and into the northern Lau and North Fiji Basins) during the West-to-East "drive by" [*Hart et al*., 2004] (Figure 8) of the northern terminus of the Tonga Trench. Furthermore, *Phipps-Morgan et al*. [1995] found that residue from hot spot melting, which forms a restite "root" at the base of the lithosphere, has lower density than ambient mantle. Owing, in part, to the lower density, the restite root will spread laterally, or "pancake," at the base of the lithosphere over a period of at least 50 My following melt extraction. In the case of Samoa, lateral spreading of the plume restite may permit some of the flattening restite to extend south of the Vitiaz Lineament. Together with slab-induced toroidal flow, the lateral spreading due to pancaking of the plume will help advect the Samoan plume keel into the northern Lau and North Fiji Basins.

Additionally, starting at ~2 Ma, the older portions of two hot spots now active in the Cook Austral volcanic lineaments—first the Rarotonga hot spot trace, followed by the Rurutu hot spot—began subducting into the Tonga Trench, thereby contributing their geochemical signatures to the northern Lau Basin. Below, we explore how these geodynamic processes occurred in three time steps (at 4 Ma, 2 Ma, and the present) as well as how they may have contributed to the formation of the geochemical patterns observed in the Lau and North Fiji basins today.

We note that our conceptual model for mantle flow in the Lau and North Fiji basins has fundamental limitations: the geodynamics of mantle flow around slab edges are highly uncertain and time-dependent owing to a variety of poorly constrained parameters that include the possible thermal influence from the Samoan plume [e.g., *Putirka*, 2008], mantle wedge and plume restite viscosity, roll back rate, slab strength, etc. [e.g., *Phipps-Morgan et al*., 1995; *Jadamec and Billen*, 2016; *Druken et al*., 2011, 2014].

5.1.1. The Geodynamic Picture at ~4 Ma: Incorporation of Advected Samoan Underplated Plume Mantle

The trace of the Samoan hot spot track is known to extend westward to Alexa Bank, a 24 million year old seamount located ~1700 km west of the active Samoan hot spot [*Hart et al*., 2004] (but we note that the Samoan hot spot may have been active for over 100 Ma, *Koppers et al*. [2003]). Previously published isotopic data on lavas from the North Fiji Basin [*Price et al*., 2014] suggest that an enriched mantle component (similar to that found in the Samoan hot spot) influenced the composition of the mantle beneath South Pandora Ridge (which is anchored by Rotuma at its eastern terminus; Figure 1). This is a notable finding, given that the Samoan hot spot is located ~1700 km to the east of South Pandora Ridge (Figure 1) [*Price et al*., 2014]. Based on plate reconstruction models from *Wessel and Kroenke* [2008], and the tectonic reconstruction of *Hart et al*. [2008], Figure 8 illustrates that, at 4 Ma, Samoa was the only hot spot track in the region that was likely to contribute geochemically enriched signatures to the North Fiji Basin near South Pandora Ridge and Rotuma. This is because the trace of the Samoan hot spot runs along the length of the northern border of

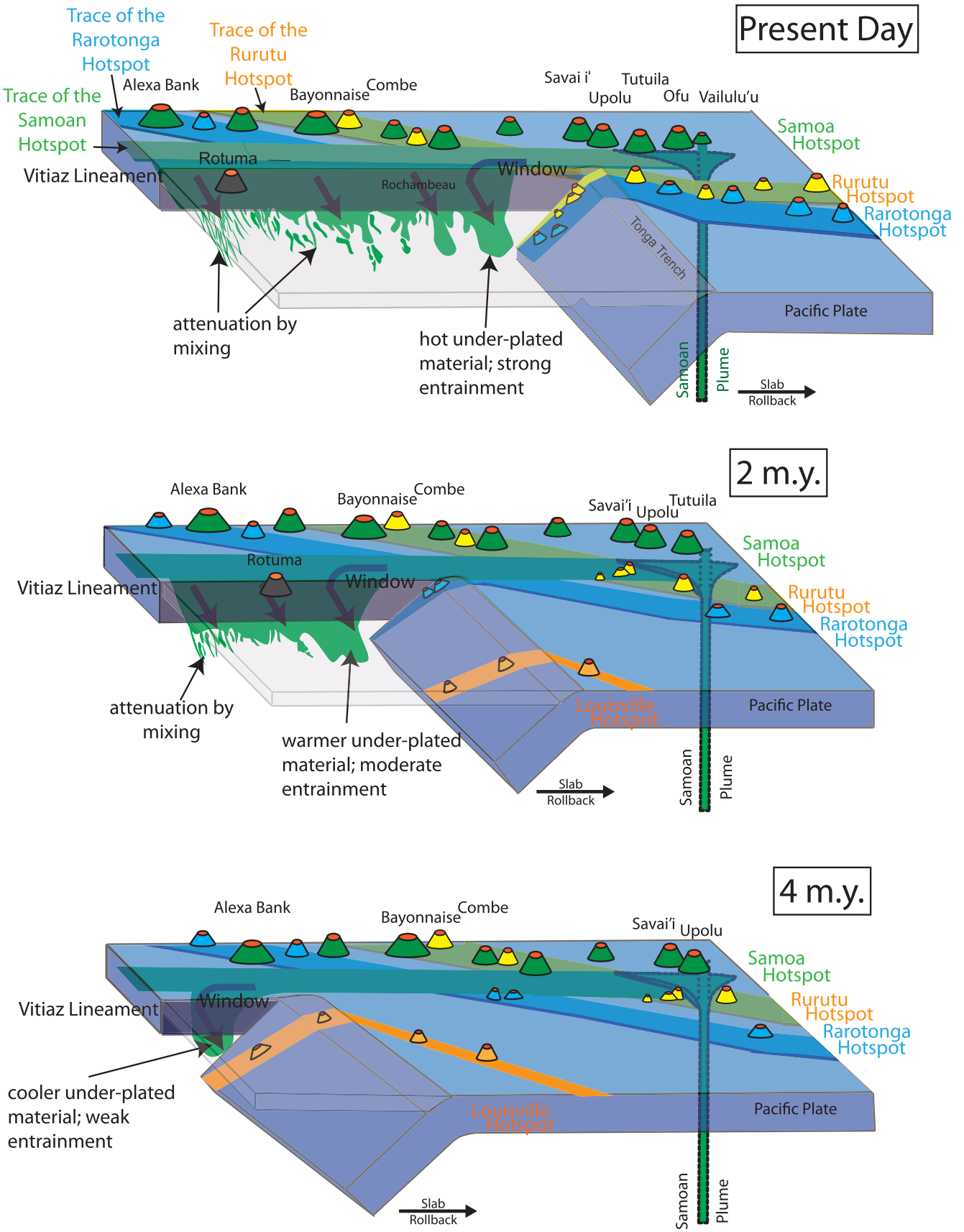
Present Day
Trace of the Rarotonga Hotspot
Trace of the Rurutu Hotspot
Trace of the Samoan Hotspot
Alexa Bank
Bayonnaise
Combe
Savai i'
Tutuila
Upolu
Ofu
Vailulu'u
Samoa Hotspot
Rotuma
Vitiaz Lineament
Rochambeau
Window
Rurutu Hotspot
Rarotonga Hotspot
Tonga Trench
attenuation by mixing
hot under-plated material; strong entrainment
Pacific Plate
Samoan Plume
Slab Rollback
2 m.y.
Alexa Bank
Bayonnaise
Combe
Savai'i
Upolu
Tutuila
Samoa Hotspot
Rotuma
Vitiaz Lineament
Window
Rurutu Hotspot
Rarotonga Hotspot
attenuation by mixing
warmer under-plated material; moderate entrainment
Louisville Hotspot
Pacific Plate
Slab Rollback
Samoan Plume
4 m.y.
Alexa Bank
Bayonnaise
Combe
Savai'i
Upolu
Samoa Hotspot
Vitiaz Lineament
Window
Rurutu Hotspot
Rarotonga Hotspot
cooler under-plated material; weak entrainment
Louisville Hotspot
Pacific Plate
Slab Rollback
Samoan Plume

the Lau and North Fiji Basins, and no other geochemically enriched hot spots are located near the Pandora Ridge at 4 Ma. New and previously published data on lavas from the Fiji Triple Junction exhibit geochemically enriched isotopic signatures similar to those identified in the South Pandora Ridge (Figures 2 and 3), unlike the geochemical signature typical of back-arc basins, suggesting a role for the incursion of Samoan plume material further south of South Pandora Ridge. Indeed, a series of binary mixing models between several depleted Lau and North Fiji Basin components and five Samoan plume components [*Jackson et al*., 2014] capture much of the radiogenic isotopic variability in South Pandora Ridge lavas and other North Fiji Basin lavas (e.g., Fiji Triple Junction, Yasawa-Yadua Volcanic Zone, and West Cikobia Volcanic Zone) (see supporting information Text S1, Table S3, and Figure S3). This result supports a model where components associated with the Samoan hot spot have been advected into the North Fiji Basin and sampled by mantle melting.

Figure 8 shows that, at 4 Ma, the northern terminus of the Tonga Trench was located just south of Alexa Bank, a seamount of Samoan isotopic pedigree that was ~20 million years old (i.e., 24 Ma minus 4 Ma) at this time interval [*Hart et al*., 2004]. Thus, at 4 Ma, underplated Samoan plume material (i.e., underplated on the Pacific mantle lithosphere beneath Alexa) that was available for entrainment by toroidal flow around the slab edge and into the Fiji Basin was ~20 million years old. However, underplated Samoan plume material located closer to the active hot spot should be hotter, because it has had less time to cool by diffusive heat loss. Thus, older underplated plume material would be cooler and more viscous, and less easily entrained by toroidal flow, relative to the younger, warmer underplated Samoan plume material (located closer to the Samoan plume) that is currently being entrained by the toroidal flow around the slab edge into the Lau Basin (see below). Furthermore, the *Phipps-Morgan et al*. [1995] model would predict that older plume restite under Alexa would pancake and spread laterally at a slower rate than younger plume restite located closer to the Samoan hot spot, which would further slow southward advection of underplated Samoan plume material near Alexa.

Another hot spot track in the southwest Pacific, the Louisville hot spot track, has also been suggested as a contributor to the mantle heterogeneity observed in the Lau back-arc basin [e.g., *Turner and Hawkesworth*, 1998; *Ewart et al*., 1998]. Louisville hot spot subduction began at ~4 Ma, coinciding with the opening of the Lau Basin, and the location of subduction of the Louisville hot spot track into the Tonga Trench has swept southward over the past 4 Ma [*Ruellan et al*., 2003]. *Timm et al*. [2013] showed that there is a geochemical influence from the subduction of the Louisville hot spot track in the southern Lau backarc, near the present-day locus of subduction of the Louisville hot spot track. However, there is no indication in existing data sets for the presence of a Louisville geochemical signature in lavas from the northern Lau backarc [*Price et al*., 2016] (see section 5.1.3, for further discussion of Louisville subduction).

5.1.2. The Geodynamic Picture at ~2 Ma: Initiation of Subduction of the Rarotonga Hot Spot Track into the Tonga Trench and Enhanced Entrainment of Samoan Underplated Material

At 4 Ma, the only other enriched mantle hot spot track in the region, the Rarotonga hot spot track, was located to the northeast of the northern terminus of the Tonga Trench (based on the plate reconstruction of *Wessel and Kroenke* [2008]) (Figure 8) and was unlikely to contribute to the geochemical enrichment observed in the North Fiji Basin (Figures 5 and 7). However, by ~2 Ma, the trace of the Rarotonga hot spot track would have intersected first with the northern portion of the eastward-migrating Tonga Trench which, at the time, was located just south of Combe seamount (see Figure 8). Thus, from ~2 Ma to the present, subducted seamounts from the older portion of the Rarotonga hot spot track would have subducted into the Tonga Trench, thereby contributing distinct, geochemically enriched signatures to the back-arc basin:

Figure 8. Cartoon schematic showing the tectonic evolution of the Lau and North Fiji Basins over the past 4 million years, based on a three-dimensional adaptation of Figure 9 from *Hart et al*. [2004]. As the Tonga trench has migrated to the east relative to the Samoan hot spot over the past 4 Ma, underplated Samoan-plume material has been drawn into the northern Lau and North Fiji Basins by toroidal flow around the Tonga slab. As the tear in the Pacific plate neared the Samoan hot spot, the underplated Samoan-plume material entrained by toroidal flow (the curved arrow) is progressively younger, and therefore hotter and less viscous, and easier to entrain. As a result, there is enhanced entrainment of Samoan material by toroidal flow around the slab at the present day compared to 4 Ma, resulting in clearer/stronger Samoan plume signatures (higher $^{87}Sr/^{86}Sr$ and higher maximum $^{3}He/^{4}He$) in the northeast Lau Basin compare to the 4 Ma and 2 Ma timesteps. Also, any geochemical signatures associated with Samoan plume material entrained into the North Fiji Basin (at ~4 Ma) have had more time to mix with ambient depleted mantle, resulting in weaker (more attenuated) Samoan plume signatures in the west. Additionally, we show that, by ~2 Ma, the Rarotonga hot spot track began subducting into the Tonga Trench, and continues to subduct into the present day. The Rurutu Hot spot track also begins to subduct into the Tonga Trench during the most recent time interval (2 Ma to present). The Louisville hot spot track is shown in the 4 Ma and 2 Ma time steps; it plots off (below) the cartoon in the present day timestep because it is currently subducting further to the south (beneath the Southern Lau Basin). The locations of Lau Basin back-arc spreading centers at 2 Ma and 4 Ma are not included owing to uncertainty in their paleolocations.

The Rarotonga hot spot track has geochemically enriched $^{87}Sr/^{86}Sr$, including lavas with $^{87}Sr/^{86}Sr$ up to 0.70488 (sample AIT-64A from Aitutaki Island—related to the Rarotonga hot spot [e.g., *Chauvel et al*., 1997]—from *Nakamura and Tatsumoto* [1988]) and 0.705222 (sample 16-95-2 from Uo Mamae Seamount from *Pearce et al*. [2007]). Thus, geochemically enriched hot spot signatures from the subducting Rarotonga hot spot track, if present in the Lau Basin, would be apparent in the back-arc basin mantle south of Combe (including the East Futuna Volcanic Zone and Futuna Central Zone), but not in the region of the back-arc basin to the west. However, due to continued subduction of the Rarotonga hot spot from 2 Ma to the present, a broad swath of the Lau Basin, from the region south of Combe eastward to the back-arc mantle at the Northeast Lau Basin and Fonualei Rift and Spreading Center, may host an enriched geochemical signature from the Rarotonga hot spot. Consistent with this hypothesis, more geochemically enriched $^{87}Sr/^{86}Sr$ appears in the Lau Basin in the region south of Combe and the magnitude of the enriched signature is enhanced to the east (Figure 5).

The subducting Rarotonga hot spot track, however, was not the only contributor of enriched geochemical signatures, including high $^{87}Sr/^{86}Sr$, to the northern Lau Basin. Compared to toroidal entrainment of Samoan plume material at 4 Ma (when the northern terminus was located just south of Rotuma), there may have been enhanced entrainment of enriched underplated Samoan plume material by toroidal flow around the slab edge by 2 Ma. This is because the northern terminus of the Tonga Trench was located just south of the 11 Ma Combe Bank [*Hart et al*., 2004; *Koppers et al*., 2011] which, at 2 Ma, was only ~9 million years old. The underplated Samoan plume material beneath Combe was younger, warmer, and therefore less viscous than the ~20 million year old underplated Samoan plume material advected beneath Alexa seamount at the 4 Ma time interval. In this way, a greater contribution from the Samoan plume, and therefore clearer Samoan geochemical signatures (i.e., higher maximum $^{87}Sr/^{86}Sr$), would be available in the northern Lau Basin at ~2 Ma compared to the North Fiji Basin at ~4 Ma. Due to warmer temperatures and lower viscosity, pancaking (and associated southward spreading) of the underplated Samoan plume also would have occurred at a faster rate. Thus, we suggest that the stronger signatures of geochemical enrichment (i.e., higher $^{87}Sr/^{86}Sr$) found in the Lau Basin east of 178°W (i.e., the longitude of Combe) may be related to a contribution from two distinct EM hot spots, including the first appearance of subducted Rarotonga material at ~2 Ma and enhanced southward advection of younger, hotter and less viscous underplated Samoa plume material. However, we note that much of the geochemical variability identified in the northern Lau Basin (excluding the northeast Lau Basin) can be explained by binary mixing of geochemical components associated with the Samoan hot spot and geochemically depleted back-arc basin components (see supporting information Text S1 and Figure S3), and it is only in the northeast Lau Basin that that a clear role for input from the Rarotonga hot spot is observed [*Price et al*., 2016].

5.1.3. Implications of Continued Pacific Slab Rollback to the Present Day

The most geochemically enriched lavas yet discovered in the study region are found in the northeastern Lau Basin. We argue that the strongly enriched geochemical signatures seen in the northeastern Lau Basin relate to the present-day tectonic configuration of the Pacific plate and the plates that comprise the Lau Basin, the subducting hot spots from the Cook-Austral volcanic lineament, and the Samoan plume. While the northern terminus of the Tonga Trench currently is closer to the Samoan plume than at any other time in its history, the 400 km distance may still be too great to directly entrain material from the upwelling Samoan plume conduit into the Lau Basin via toroidal flow around the subducting Tonga slab. Indeed, the west-to-east younging of plume-derived shield volcanoes in Samoa [*Koppers et al*., 2008, 2011] is consistent with a relatively laterally stationary Samoan plume conduit, and therefore inconsistent with a 400 km east-to-west migration of the Samoan plume conduit from the hot spot (at Vailulu'u seamount) to the Lau Basin (Figure 1). However, the northern terminus of the Tonga Trench is presently located only ~150 km south of the island of Savai'i, which has shield-stage lavas of only ~4–5 Ma of age [*Koppers et al*., 2011]. Thus, underplated Samoan plume material attached to the Pacific lithosphere beneath Savai'i is young (only 4 to 5 Ma), and therefore younger, hotter and less viscous than the putative underplated Samoan plume material entrained by slab rollback at the 2 and 4 Ma time steps in our model (shown in Figure 8). As a result, underplated Samoan plume material currently being entrained into the Lau Basin should be more easily entrained by toroidal flow (and more easily advected southward by plume restite pancaking, *Phipps-Morgan et al*. [1995]) than underplated Samoan plume material entrained in the prior 4 million year history of basin opening. This predicts stronger signatures of geochemical enrichment in the northern Lau Basin associated with entrainment of underplated Samoan plume material. Indeed, the presence of boninites found in the

northeastern Lau Basin [e.g., *Sobolev and Danyushevsky*, 1994; *Falloon and Danyushevsky*, 2000; *Resing et al*., 2011], closest to the Samoan plume, is consistent with elevated temperatures (as high as ~1480°C) in the mantle wedge above the northern Tonga slab, and points to incursion of young, hot Samoan plume material into the Lau Basin [*Sobolev and Danyushevsky*, 1994; *Falloon and Danyushevsky*, 2000].

While enhanced signatures of geochemical enrichment in the northeastern region of the Lau Basin (Figures 5 and 7) may be attributable to more efficient entrainment of progressively younger and hotter underplated Samoan plume material as the Tonga Trench approaches Samoa, additional factors are likely at play. For example, underplated Samoan plume material that was swept into the Lau Basin at 4 Ma has had more time to mix with ambient depleted back-arc basin mantle than Samoan plume material that was more recently incorporated into the Lau Basin from beneath Savai'i. Thus, geochemically enriched Samoan plume signatures entrained at 4 Ma have had more time to mix with ambient back-arc basin mantle than more recently entrained Samoan plume signatures, and this may help explain the weaker signals of geochemical enrichment observed in the western regions of the back-arc basins compared to the eastern regions (Figures 5 and 7).

In addition to the incorporation of Samoan mantle material, and the continual subduction of the Rarotonga hot spot track under the northern Lau Basin, geochemical data and hot spot track reconstructions show evidence for recent (<1 Ma) initiation of subduction of the HIMU Rututu hot spot track under the northeastern Lau Basin. The most extreme high $^{206}Pb/^{204}Pb$ ratios are confined to the northeastern portion of the Lau Basin, adjacent to the intersection of the Rurutu hot spot track and the Tonga Trench (Figure 7). Unlike Samoan hot spot material (which has been incorporated in the Lau and North Fiji Basins for the past 4–5 Ma) and the Rarotonga hot spot (which was introduced via subduction at ~2 Ma), the HIMU signature from Rurutu was only recently introduced into the Lau Basin. Therefore, the HIMU influence is more geographically restricted than the influence from the other hot spots, and the HIMU signature is only visible in the northeast Lau Basin (Figure 7).

We also note that a contribution from the subducted Louisville hot spot has been suggested for lavas in the northern Tonga Arc [e.g., *Wendt et al*., 1997; *Turner and Hawkesworth*, 1998; *Regelous et al*., 2008; *Beier et al*., 2011]. This link is made because northern Tonga Arc lavas, especially from Niuatoputapu and Tafahi Islands, exhibit moderately radiogenic Pb isotopic signatures that are suggested to reflect the radiogenic Pb observed in Louisville hot spot volcanoes. However, the locus of Louisville hot spot subduction has swept southward, away from the northernmost Tonga Trench, over the past ~4 million years [*Ruellan et al*., 2003]. We note that seamounts associated with the older portion of a HIMU Cook-Austral hot spot (the Rurutu hot spot) are suggested to currently be subducting under the northern Tonga Arc, thereby explaining the radiogenic Pb isotopic signatures in the Northern Lau Basin [*Falloon et al*., 2007; *Price et al*., 2016]. The HIMU signature from the Rurutu hot spot may also contribute radiogenic Pb to the northern Tonga Arc, in lieu of a contribution from the Louisville hot spot. While we do not rule out a contribution from Louisville in the Tonga arc, we note that Rurutu is a plausible end-member for the unusual radiogenic isotopic compositions of these arc lavas, particularly if these lavas are a result of mixing a Tonga arc component with a Rurutu hot spot component. Supporting this hypothesis, the northern Tonga Arc volcanoes of Niuatoputapu and Tafahi Islands plot between the fields for Rurutu hot spot lavas and Tonga arc lavas in all radiogenic isotopic spaces (see supporting information Figure S3).

5.2. Formation of North-South Geochemical Gradients in the Lau and North Fiji Basins

In addition to the east-west geochemical gradients discussed above, strong north-south geochemical gradients are also observed in the Lau and North Fiji Basins. Across the Lau and North Fiji Basins, the most geochemically enriched lavas are found in the north, and these enriched geochemical signatures decrease to background, depleted back-arc basin signatures in the south (Figure 5). We hypothesize that this is because all known geochemically enriched hot spot-related signatures—the Samoan hot spot and the Rarotonga hot spot—enter the Lau and North Fiji Basins from the north (Figures 1 and 8): underplated Samoan hot spot material enters the Lau and North Fiji basins from the northern fringes of the region, and the Rarotonga hot spot has been subducted into the northern Tonga Trench over the past 2 Ma and supplies geochemically enriched signatures to the Lau Basin from the north (Figure 8). Therefore, the strongest geochemically enriched signals are incorporated into the basins in the northern regions. These geochemically enriched signatures are likely attenuated, by mixing with ambient depleted back-arc basin mantle, as the enriched

mantle materials are advected to the south in the broad north-to-south mantle flow suggested in the region [*Pearce et al*., 2007].

6. Conclusions

First, we find that strong zonal and meridional geochemical patterns exist within the region, and these patterns can be explained by the incorporation of three different Pacific hot spots via different processes over the past 4 Ma. Second, we argue that the incorporation of underplated Samoan mantle material via toroidal flow around the subducting Pacific Plate, and via pancaking and southward spreading of underplated Samoan plume restite, likely has occurred over the past ~4 Ma. Stronger Samoan geochemical signatures are seen in the eastern Lau Basin compared to the northern North Fiji Basin as the younger, hotter, and less viscous Samoan underplated material located in the east is more easily advected to the south than the older, colder, more viscous underplated Samoan material located to the west. Third, the weaker signals of geochemical enrichment observed in the western regions of the back-arc basins compared to the eastern regions may be due to longer periods of mixing with depleted ambient back-arc basin mantle, which will serve to more severely attenuate entrained Samoan hot spot signatures in the west. Fourth, a plate reconstruction suggests that, although the subduction of the Rarotonga Hot spot track by ~2 Ma can help explain high $^{87}Sr/^{86}Sr$ in lavas in the Lau Basin in conjunction with addition of a Samoan component by toroidal flow over this time interval, only Samoan underplated material can account for the enriched geochemical signatures in the North Fiji Basin. Fifth, we find that the most radiogenic Sr (EM) and Pb (HIMU) isotopic compositions in the Lau and North Fiji Basin lavas are limited to the northeastern Lau Basin; these patterns of geochemical enrichment are likely related to the recent initiation of subduction of the Rurutu and Rarotonga hot spot tracks beneath the northeast Lau Basin (at ~1 Ma and ~2 Ma, respectively), as well as enhanced southward advection of younger, hotter underplated Samoan plume material. Finally, we find that north-south gradients in both the Lau and North Fiji Basins are most enriched in the northern portions of the basin, and become more depleted southward. These gradients are likely due to the fact that the sources of enriched material to both basins are located to the north; any enriched material that is advected southward is mixed with the ambient depleted mantle, thereby attenuating enriched geochemical signatures toward the south.

Acknowledgments

MGJ acknowledges NSF grants EAR-1624840, EAR-1348082, and EAR-1347377. JBT acknowledges financial support from the French Agence Nationale de la Recherche through grant ANR-10-BLAN-0603 (M&Ms—Mantle Melting—Measurements, Models, Mechanisms). MDK acknowledges NSF support for the noble gas laboratory at WHOI (via OCE-1232985 and OCE −1259218) and the noble gas analytical efforts of Joshua Curtice. FEJ acknowledges funding from the Deep Carbon Observatory (DCO). We also thank Paul Hall for insightful discussions and two unnamed reviewers for their helpful comments.

References

Beier, C., L. Vanderkluysen, M. Regelous, J. J. Mahoney, and D. Garbe-Schönberg (2011), Lithospheric control on geochemical composition along the Louisville Seamount Chain, *Geochem. Geophys. Geosyst.*, *12*, Q0AM01, doi:10.1029/2011GC003690.

Blichert-Toft, J., and F. Albarède (1997), The Lu-Hf isotope geochemistry of chondrites and the evolution of the mantle-crust system, *Earth Planet. Sci. Lett.*, *148*, 243–258.

Blichert-Toft, J., and F. Albarède (2009), Mixing of isotopic heterogeneities in the Mauna Kea plume conduit, *Earth Planet. Sci. Lett.*, *282*(1), 190–200.

Blichert-Toft, J., C. Chauvel, and F. Albarede (1997), Separation of Hf and Lu for high-precision isotope analysis of rock samples by magnetic sector-multiple collector ICP-MS, *Contrib. Mineral. Petrol.*, *127*, 248–260.

Boespflug, X., L. Dosso, H. Bougault, and J. Joron (1990), Trace element and isotopic (Sr, Nd) geochemistry of volcanic rocks from the Lau Basin, *Geol. Jahrb. Reihe D Heft*, *92*, 1–14.

Bonneville, A., L. Dosso, and A. Hildenbrand (2006), Temporal evolution and geochemical variability of the South Pacific superplume activity, *Earth Planet. Sci. Lett.*, *244*, 251–269, doi:10.1016/j.epsl.2005.12.037.

Caulfield, J. T., S. P. Turner, I. E. M. Smith, L. B. Cooper, and G. A. Jenner (2012), Magma evolution in the primitive, intra-oceanic Tonga arc: Petrogenesis of basaltic andesites at Tofua volcano, *J. Petrol.*, *53*(6), 1197–1230.

Caulfield, J., J. Blichert-Toft, F. Albarede, and S. Turner (2015), Corrigendum to "Magma evolution in the primitive, intra-oceanic Tonga arc: Petrogenesis of Basaltic Andesites at Tofua Volcano" and 'Magma evolution in the Primitive, Intra-oceanic Tonga arc: Rapid Petrogenesis of Dacites at Fonualei Volcano', *J. Petrol.*, *56*(3), 641–644.

Chauvel, C., A. W. Hofmann, and P. Vidal (1992), HIMU-EM: The French Polynesian connection, *Earth Planet. Sci. Lett.*, *110*(1–4), 99–119.

Chauvel, C., W. F. McDonough, G. Guille, R. Maury, and R. Duncan (1997), Contrasting old and young volcanism in Rurutu Island, Austral chain, *Chem. Geol.*, *139*(1–4), 125–143.

Cheng, Q., K.-H. Park, J. D. Macdougall, A. Zindler, G. W. Lugmair, H. Staudigel, J. Hawkins, and P. Lonsdale (1987), Isotopic evidence for a hotspot origin of the Louisville seamount chain, in *Seamounts, Islands, and Atolls*, edited by B. H. Keating, et al., AGU, Washington, D. C., doi:10.1029/GM043p0283.

Condomines, M., K. Grönvold, P. Hooker, K. Muehlenbachs, R. O'Nions, N. Oskarsson, and E. R. Oxburgh (1983), Helium, oxygen, strontium and neodymium isotopic relationships in Icelandic volcanics, *Earth Planet. Sci. Lett.*, *66*, 125–36.

Danyushevsky, L. V., A. V. Sobolev, and T. J. Falloon (1995), North Tongan high-Ca boninite petrogenesis: The role of Samoan plume and subduction zone-transform fault transition, *J. Geodyn.*, *20*(3), 219–241.

Druken, K. A., M. D. Long, and C. Kincaid (2011), Patterns in seismic anisotropy driven by rollback subduction beneath the High Lava Plains, *Geophys. Res. Lett.*, *38*, L13310, doi:10.1029/2011GL047541.

Druken, K. A., C. Kincaid, R. W. Griffiths, D. R. Stegman, and S. R. Hart (2014), Plume–slab interaction: The Samoa–Tonga system, *Phys. Earth Planet. Inter.*, *232*, 1–14.

Eisele, J., W. Abouchami, S. J. Galer, and A. W. Hofmann (2003), The 320 kyr Pb isotope evolution of Mauna Kea lavas recorded in the HSDP-2 drill core, *Geochem. Geophys. Geosyst.*, *4*(5), 8710, doi:10.1029/2002GC000339.

Escrig, S., A. Bézos, S. L. Goldstein, C. H. Langmuir, and P. J. Michael (2009), Mantle source variations beneath the Eastern Lau Spreading Center and the nature of subduction components in the Lau basin–Tonga arc system, *Geochem. Geophys. Geosyst.*, *10*, Q04014, doi:10.1029/2008GC002281.

Escrig, S., A. Bézos, C. H. Langmuir, P. J. Michael, and R. Arculus (2012), Characterizing the effect of mantle source, subduction input and melting in the Fonualei Spreading Center, Lau Basin: Constraints on the origin of the boninitic signature of the back-arc lavas, *Geochem. Geophys. Geosyst.*, *13*, Q10008, doi:10.1029/2012GC004130.

Ewart, A., K. D. Collerson, M. Regelous, J. I. Wendt, and Y. Niu (1998), Geochemical evolution within the Tonga-Kermadec-Lau arc-back-arc systems: The role of varying mantle wedge composition in space and time, *J. Petrol.*, *39*, 331–368.

Falloon, T. J., and A. J. Crawford (1991), The petrogenesis of high-calcium boninite lavas dredged from the northern Tonga ridge, *Earth Planet. Sci. Lett.*, *102*(3), 375–394.

Falloon, T. J., and L. V. Danyushevsky (2000), Melting of refractory mantle at 1· 5, 2 and 2· 5 GPa under anhydrous and H^2O-undersaturated conditions: Implications for the petrogenesis of high-Ca boninites and the influence of subduction components on mantle melting, *J. Petrol.*, *41*(2), 257–283.

Falloon, T. J., L. V. Danyushevsky, T. J. Crawford, R. Maas, J. D. Woodhead, S. Eggins, S. H. Bloomer, D. J. Wright, S. K. Zlobin, and A. R. Stacey (2007), Multiple mantle plume components involved in the petrogenesis of subduction-related lavas from the northern termination of the Tonga Arc and northern Lau Basin: Evidence from the geochemistry of arc and backarc submarine volcanics, *Geochem. Geophys. Geosyst.*, *8*, Q09003, doi:10.1029/2007GC001619.

Falloon, T. J., L. V. Danyushevsky, A. J. Crawford, S. Meffre, J. D. Woodhead, and S. H. Bloomer (2008), Boninites and adakites from the northern termination of the Tonga Trench: Implications for adakite petrogenesis, *J. Petrol.*, *49*(4), 697–715.

Farley, K. A., J. Natland, and H. Craig (1992), Binary mixing of enriched and undegassed (primitive?) mantle components (He, Sr, Nd, Pb) in Samoan lavas, *Earth Planet. Sci. Lett.*, *111*, 183–199.

French, S. W., and B. Romanowicz (2015), Broad plumes rooted at the base of the Earth's mantle beneath major hotspots, *Nature*, *525*(7567), 95–99.

Fretzdorff, S., U. Schwarz-Schampera, H. L. Gibson, C. D. Garbe-Schönberg, F. Hauff, and P. Stoffers (2006), Hydrothermal activity and magma genesis along a propagating back-arc basin: Valu Fa Ridge (southern Lau Basin), *J. Geophys. Res.*, *111*, B08205, doi:10.1029/2005JB003967.

Füri, E., D. Hilton, S. Halldórsson, P. Barry, D. Hahm, T. Fischer, and K. Grönvold (2010), Apparent decoupling of the He and Ne isotope systematics of the Icelandic mantle: The role of He depletion, melt mixing, degassing fractionation and air interaction, *Geochim. Cosmochim. Acta*, *74*, 3307–3332.

Gale, A., C. A. Dalton, C. H. Langmuir, Y. Su, and J. G. Schilling (2013), The mean composition of ocean ridge basalts, *Geochem. Geophys. Geosyst.*, *14*, 489–518, doi:10.1029/2012GC004334.

Garcia, M. O., D. Hanano, A. Flinders, D. Weis, G. Ito, and M. D. Kurz (2012), Age, geology, geophysics, and geochemistry of Mahukona Volcano, Hawaii, *Bull. Volcanol.*, *74*, 1445–1463.

Georgen, J. E., M. D. Kurz, H. J. Dick, and J. Lin (2003), Low 3 He/4 He ratios in basalt glasses from the western Southwest Indian Ridge (10°–24° E), *Earth Planet. Sci. Lett.*, *206*(3), 509–528.

Gill, J. B. (1984), Sr-Pb-Nd isotopic evidence that both MORB and OIB sources contribute to ocean island arc magmas in Fiji, *Earth Planet. Sci. Lett.*, *68*, 443–458.

Gill, J., and P. Whelan (1989), Postsubduction ocean island alkali basalts in Fiji, *J. Geophys. Res.*, *94*(B4), 4579–4588.

Graham, D. W., D. M. Christie, K. S. Harpp, and J. E. Lupton (1993), Mantle plume helium in submarine basalts from the Galápagos platform, *Science*, *262*(5142), 2023–2026.

Graham, D. W., L. M. Larsen, B. B. Hanan, M. Storey, A. K. Pedersen, and J. E. Lupton (1998), Helium isotope composition of the early Iceland mantle plume inferred from the Tertiary picrites of West Greenland, *Earth Planet. Sci. Lett.*, *160*(3), 241–255.

Graham, D. W. (2002), Noble gas isotope geochemistry of mid-ocean ridge and ocean island basalts: Characterization of mantle source reservoirs, *Rev. Mineral. Geochem.*, *47*(1), 247–317.

Haase, K. M., T. J. Worthington, P. Stoffers, D. Garbe-Schönberg, and I. Wright (2002), Mantle dynamics, element recycling, and magma genesis beneath the Kermadec Arc-Havre Trough, *Geochem. Geophys. Geosyst.*, *3*(11), 1071, doi:10.1029/2002GC000335.

Haase, K. M., S. Fretzdorff, R. Mühe, D. Garbe-Schönberg, and P. Stoffers (2009), A geochemical study of off-axis seamount lavas at the Valu Fa Ridge: Constraints on magma genesis and slab contributions in the southern Tonga subduction zone, *Lithos*, *112*, 137–148, doi:10.1016/j.lithos.2009.05.041.

Hahm, D., D. R. Hilton, P. R. Castillo, et al. (2012), An overview of the volatile systematics of the Lau Basin: Resolving the effects of source variation, magmatic degassing and crustal contamination, *Geochim. Cosmochim. Acta*, *85*, 88–113, doi:10.1016/j.gca.2012.02.007.

Hamilton, P. J., et al. (1983), Sm-Nd studies of Archaean metasediments and metavolcanics from West Greenland and their implications for the Earth's early history, *Earth Planet. Sci. Lett.*, *62*(2), 263–272.

Hanyu, T., Y. Tatsumi, R. Senda, et al. (2011), Geochemical characteristics and origin of the HIMU reservoir: A possible mantle plume source in the lower mantle, *Geochem. Geophys. Geosyst.*, *12*, Q0AC09, doi:10.1029/2010GC003252.

Hart, S. (1984), A large-scale isotope anomaly in the Southern Hemisphere mantle, *Nature*, *309*, 753–757.

Hart, S., and J. Blusztajn (2006), Age and geochemistry of the mafic sills, ODP site 1276, Newfoundland margin, *Chem. Geol.*, *235*, 222–237, doi:10.1016/j.chemgeo.2006.07.001.

Hart, S. R., and M. G. Jackson (2014), Evolution of Ta'u and Ofu/Olosega volcanoes—The "Twin Sisters" of Samoa, *Geochem. Geophys. Geosyst.*, *15*, 2301–2318, doi:10.1002/2013GC00522.

Hart, S. R., M. Coetzee, R. K. Workman, J. Blusztajn, K. T. M. Johnson, J. M. Sinton, B. Steinberger, and J. W. Hawkins (2004), Genesis of the Western Samoa seamount province: Age, geochemical fingerprint and tectonics, *Earth Planet. Sci. Lett.*, *227*(1), 37–56.

Harvey, J., and E. F. Baxter (2009), An improved method for TIMS high precision neodymium isotope analysis of very small aliquots (1–10 ng), *Chem. Geol.*, *258*(3), 251–257.

Hauri, E. H., and S. Hart (1993), Re-Os isotope systematics of HIMU and EMII oceanic island basalts from the south Pacific Ocean, *Earth Planet. Sci. Lett.*, *114*, 353–371.

Hedman, K. M., B. B. Curry, T. M. Johnson, P. D. Fullagar, and T. E. Emerson (2009), Variation in strontium isotope ratios of archaeological fauna in the Midwestern United States: A preliminary study, *J. Archaeol. Sci.*, *36*(1), 64–73.

Hemond, C., C. Devey, and C. Chauvel (1994), Source compositions and melting processes in the Society and Austral plumes (South Pacific Ocean): Element and isotope (Sr, Nd, Pb, Th) geochemistry, *Chem. Geol.*, 7–45.

Hergt, J., and J. D. Woodhead (2007), A critical evaluation of recent models for Lau-Tonga arc-backarc basin magmatic evolution, *Chem. Geol.*, *245*, 9–44, doi:10.1016/j.chemgeo.2007.07.022.

Hilton, D. R., K. Hammerschmidt, G. Loock, and H. Friedrichsen (1993), Helium and argon isotope systematics of the central Lau Basin and Valu Fa Ridge: Evidence of crust/mantle interactions in a back-arc basin, *Geochim. Cosmochim. Acta*, *57*, 2819–2841.

Hilton, D. R., K. Grönvold, C. G. Macpherson, and P. R. Castillo (1999), Extreme 3He/4He ratios in Iceland: Constraining the common component in mantle plumes, *Earth Planet Sci Lett.*, *173*, 53–60.

Hofmann, A. W., and W. M. White (1982), Mantle plumes from ancient oceanic crust, *Earth Planet. Sci. Lett.*, *57*(2), 421–436.

Honda, M., D. B. Patterson, I. McDougall, and T. J. Falloon (1993), Noble gases in submarine pillow basalt glasses from the Lau Basin: Detection of a solar component in backarc basin basalts, *Earth Planet. Sci. Lett.*, *120*, 135–148.

Jackson, M. G., and S. Hart (2006), Strontium isotopes in melt inclusions from Samoan basalts: Implications for heterogeneity in the Samoan plume, *Earth Planet. Sci. Lett.*, *245*, 260–277, doi:10.1016/j.epsl.2006.02.040.

Jackson, M. G., and R. W. Carlson (2012), Homogeneous superchondritic 142Nd/144Nd in the mid-ocean ridge basalt and ocean island basalt mantle, *Geochem. Geophys. Geosyst.*, *13*, Q06011, doi:10.1029/2012GC004114.

Jackson, M. G., S. R. Hart, A. A. P. Koppers, H. Staudigel, J. Konter, J. Blusztajn, M. Kurz, and J. A. Russell (2007a), The return of subducted continental crust in Samoan lavas, *Nature*, *448*, 684–687, doi:10.1038/nature06048.

Jackson, M. G., M. Kurz, S. Hart, and R. K. Workman (2007b), New Samoan lavas from Ofu Island reveal a hemispherically heterogeneous high $^{3}He/^{4}He$ mantle, *Earth Planet. Sci. Lett.*, *264*, 360–374, doi:10.1016/j.epsl.2007.09.023.

Jackson, M. G., S. R. Hart, A. E. Saal, N. Shimizu, M. D. Kurz, J. Blusztajn, and A. Skovgaard (2008), Globally elevated titanium, tantalum, and niobium (TITAN) in ocean island basalts with high 3He/4He, *Geochem. Geophys. Geosyst.*, *9*, Q04027, doi:10.1029/2007GC001876.

Jackson, M. G., M. D., Kurz, and S. R. Hart (2009), Helium and neon isotopes in phenocrysts from Samoan lavas: Evidence for heterogeneity in the terrestrial high 3 He/4 He mantle, *Earth Planet. Sci. Lett.*, *287*(3), 519–528.

Jackson, M. G., S. R., Hart, J. G. Konter, A. A. P. Koppers, H. Staudigel, M. D. Kurz, J. Blusztajn, and J. M. Sinton (2010), Samoan hot spot track on a "hot spot highway": Implications for mantle plumes and a deep Samoan mantle source, *Geochem. Geophys. Geosyst.*, *11*, Q12009, doi:10.1029/2010GC003232.

Jackson, M. G., S. R. Hart, J. G. Konter, M. D. Kurz, J. Blusztajn, and K. A. Farley (2014), Helium and lead isotopes reveal the geochemical geometry of the Samoan plume, *Nature*, *514*, 355–358, doi:10.1038/nature13794.

Jacobsen S. B. and G.J. Wasserburg (1980), Sm-Nd evolution of chrondrites, *Earth Planet. Sci. Lett.*, *50*, 139.

Jadamec, M. A. (2016), Insights on slab-driven mantle flow from advances in three-dimensional modelling, *J. Geodyn.*, *100*, 51–70.

Jenner, F. E., R. J. Arculus, J. A. Mavrogenes, N. J. Dyriw, O. Nebel, and E. H. Hauri (2012), Chalcophile element systematics in volcanic glasses from the northwestern Lau Basin, *Geochem. Geophys.*, *13*(6).

Jenner, G. A., P. A. Cawood, M. Rautenschlein, and W. M. White (1987), Composition of back-arc basin volcanics, Valu Fa Ridge, Lau Basin: Evidence for a slab-derived component in their mantle source, *J. Volcanol. Geotherm. Res.*, *32*(1), 209–222.

Keller, R. A., D. W. Graham, K. A. Farley, R. A. Duncan, and J. E. Lupton (2004), Cretaceous-to recent record of elevated 3He/4He along the Hawaiian-Emperor volcanic chain, *Geochem. Geophys. Geosyst.*, *5*, Q12L05, doi:10.1029/2004GC000739.

Knaack, C., S. Cornelius, and P. R. Hooper (1994), Trace element analyses of rocks and minerals by ICP-MS, *Open File Rep.*, Dep. of Geol., Washington State Univ., Pullman, Wash.

Kogiso, T., Y. Tatsumi, G. Shimoda, and H. Barsczus (1997), High u (HIMU) ocean island basalts in southern Polynesia: New evidence for whole mantle scale recycling of subducted oceanic crust, *J. Geophys. Res.*, *102*, 8085–8103.

Koppers, A. A., H. Staudigel, M. S. Pringle, and J. R. Wijbrans (2003), Short-lived and discontinuous intraplate volcanism in the South Pacific: Hot spots or extensional volcanism?, *Geochem. Geophys. Geosyst.*, *4*(10), 1089, doi:10.1029/2003GC000533.

Koppers, A. A., J. A. Russell, M. G. Jackson, J. Konter, H. Staudigel, and S. R. Hart (2008), Samoa reinstated as a primary hotspot trail, *Geology*, *36*(6), 435–438.

Koppers, A. A., J. A. Russell, J. Roberts, M. G. Jackson, J. G. Konter, D. J. Wright, H. Staudigel, and S. R. Hart (2011), Age systematics of two young en echelon Samoan volcanic trails, *Geochem. Geophys. Geosyst.*, *12*, Q07025, doi:10.1029/2010GC003438.

Kurz, M. D., and D. Geist (1999), Dynamics of the Galapagos hotspot from helium isotope geochemistry, *Geochim. Cosmochim. Acta*, *63*, 4139–56.

Kurz, M. D., W. J. Jenkins, and S. R. Hart (1982), Helium isotope systematics of ocean islands and mantle heterogeneity, *Nature*, *297*, 43–47.

Kurz, M. D., W. J. Jenkins, S. R. Hart, and D. Clague (1983), Helium isotopic variations in volcanic rocks from Loihi seamount and the island of Hawaii, *Earth Planet. Sci. Lett.*, *66*, 388–406.

Kurz, M. D., P. S. Meyer, and H. Sigurdsson (1985), Helium isotopic systematics within the neovolcanic zones of Iceland, *Earth Planet. Sci. Lett.*, *74*, 291–305.

Kurz, M. D., J., Curtice, D. E. Lott, and A. Solow (2004), Rapid helium isotopic variability in Mauna Kea shield lavas from the Hawaiian Scientific Drilling Project, *Geochem. Geophys. Geosyst.*, *5*, Q04G14, doi:10.1029/2002GC000439.

Kurz, M. D., J. Curtice, D. Fornari, D. Geist, and M. Moreira (2009), Primitive neon from the center of the Galápagos hotspot, *Earth Planet. Sci. Lett.*, *286*, 23–34.

Lackey, J. S., M. R. Cecil, C. J. Windham, R. E. Frazer, I. N. Bindeman, and G. E. Gehrels (2012), The Fine Gold Intrusive Suite: The roles of basement terranes and magma source development in the Early Cretaceous Sierra Nevada batholith, *Geosphere*, *8*(2), 292–313.

Langmuir, C. H., A. Bezos, S. Escrig, and S. W. Parman (2006), Chemical systematics and hydrous melting of the mantle in back-arc basins, in *Back-Arc Spreading Systems: Geological, Biological, Chemical, and Physical Interactions, Geophys. Monogr.*, edited by D. M. Christie, et al., vol. 166, 87 pp., AGU, Washington, D. C.

Lassiter, J. C., J. Blichert-Toft, E. H. Hauri, and H. G. Barsczus (2003), Isotope and trace element variations in lavas from Raivavae and Rapa, Cook-Austral islands: Constraints on the nature of HIMU- and EM-mantle and the origin of mid-plate volcanism in French Polynesia, *Chem. Geol.*, *202*, 115–138, doi:10.1016/j.chemgeo.2003.08.002.

Loock, G. (1990), Isotopic compositions of volcanic glasses from the Lau Basin, *Mar. Min.*, *9*, 235–246.

Lupton, J. E., R. J. Arculus, R. R. Greene, L. J. Evans, and C. I. Goddard (2009), Helium isotope variations in seafloor basalts from the Northwest Lau Backarc Basin: Mapping the influence of the Samoan hotspot, *Geophys. Res. Lett.*, *36*, L17313, doi:10.1029/2009GL039468.

Lupton, J., K. H. Rubin, R. Arculus, M. Lilley, D. Butterfield, J. Resing, E. Baker, and R. Embley (2015), Helium isotope, C/3He, and Ba-Nb-Ti signatures in the northern Lau Basin: Distinguishing arc, back-arc, and hotspot affinities, *Geochem. Geophys. Geosyst.*, *16*, 1133–1155, doi:10.1002/2014GC005625.

Lytle, M. L., K. A. Kelley, E. H. Hauri, J. B. Gill, D. Papia, and R. J. Arculus (2012), Tracing mantle sources and Samoan influence in the northwestern Lau back-arc basin, *Geochem Geophys. Geosyst.*, *13*, Q10019, doi:10.1029/2012GC004233.

Macpherson, C. G., D. R. Hilton, J. M. Sinton, R. J. Poreda, and H. Craig (1998), High 3He/4He ratios in the Manus backarc basin: Implications for mantle mixing and the origin of plumes in the western Pacific Ocean, *Geology*, *26*(11), 1007–1010.

Macpherson, C. G., D. R. Hilton, J. M. D. Day, D. Lowry, and K. Grönvold (2005), High-3He/4He, depleted mantle and low-δ18O, recycled oceanic lithosphere in the source of central Iceland magmatism, *Earth Planet. Sci. Lett.*, *233*, 411–27.

Matsuda, J., K. Notsu, J. Okano, K. Yaskawa, and L. Chungue (1984), Geochemical implications from Sr isotopes and K-Ar age determinations for the Cook-Austral Island Chain, *Tectonophysics*, *104*(1–2), 145–154.

McCulloch, M. T., and J. A. Gamble (1991), Geochemical and geodynamical constraints on subduction zone magmatism, *Earth Planet. Sci. Lett.*, *102*(3), 358–374.

Moreira, M., C. Breddam, J. Curtice, and M. D. Kurz (2001), Solar Neon in the Icelandic mantle: Evidence for an undegassed lower mantle, *Earth Planet. Sci. Lett.*, *185*, 15–23.

Müller, R. D., M. Sdrolias, C. Gaina, and W. R. Roest (2008), Age, spreading rates, and spreading asymmetry of the world's ocean crust, *Geochem. Geophys. Geosyst.*, *9*, Q04006, doi:10.1029/2007GC001743.

Mukhopadhyay, S., J. C. Lassiter, K. A. Farley, and S. W. Bogue (2003), Geochemistry of Kauai shield-stage lavas: Implications for the chemical evolution of the Hawaiian plume, *Geochem. Geophys. Geosyst.*, *4*(1), 1009, doi:10.1029/2002GC000342.

Nakamura, Y., and M. Tatsumoto (1988), Pb, Nd, and Sr isotopic evidence for a multicomponent source for rocks of Cook-Austral Islands and heterogeneities of mantle plumes, *Geochim. Cosmochim. Acta*, *52*, 2909–2924.

Nebel, O., and R. J. Arculus (2015), Selective ingress of a Samoan plume component into the northern Lau backarc basin, *Nat. Commun.*, *6*, 6554.

Nishio, Y., S. Sasaki, T. Gamo, H. Hiyagon, and Y. Sano (1998), Carbon and helium isotope systematics of North Fiji Basin basalt glasses: Carbon geochemical cycle in the subduction zone, *Earth Planet. Sci. Lett.*, *154*, 127–138.

Nohara, M., K. Hirose, J.-P. Eissen, T. Urabe, and M. Joshima (1994), The North Fiji Basin basalts and their magma sources. Part II: Sr-Nd isotopic and trace element constraints, *Mar. Geol.*, *116*, 179–195.

Pearce, J. A., and R. J. Stern (2006), Origin of back-arc basin magmas: Trace element and isotope perspectives, in *Chemical Systematics and Hydrous Melting of the Mantle in Back-Arc Basins*, edited by D. M. Christie et al., pp. 63–86, AGU, Washington, D. C.

Pearce, J. A., P. D. Kempton, and J. B. Gill (2007), Hf-Nd evidence for the origin and distribution of mantle domains in the SW Pacific, *Earth Planet. Sci. Lett.*, *260*, 98–114.

Peate, D., J. Pearce, C. Hawkesworth, H. Colley, C. M. H. Edwards, and K. Hirose (1997), Geochemical variations in Vanuatu Arc Lavas: The role of subducted material and a variable mantle wedge composition, *J. Petrol.*, *38*, 1331–1358.

Phipps Morgan, J., W. J. Morgan, and E. Price (1995), Hotspot melting generates both hotspot volcanism and a hotspot swell?. *J. Geophys. Res.*, *100*(B5), 8045–8062.

Poreda, R. J., and H. Craig (1992), He and Sr isotopes in the Lau Basin mantle: Depleted and primitive mantle components, *Earth Planet. Sci. Lett.*, *113*, 487–493.

Price, A. A., M. G. Jackson, J. Blichert-Toft, P. S. Hall, J. M. Sinton, M. D. Kurz, and J. Blusztajn (2014), Evidence for a broadly distributed Samoan-plume signature in the northern Lau and North Fiji Basins, *Geochem. Geophys. Geosyst.*, *15*, 986–1008, doi:10.1002/2013GC005061.

Price, A. A., M. G. Jackson, J. Blichert-Toft, J. Blusztajn, C. S. Conatser, J. G. Konter, A. A. Koppers, and M. D. Kurz (2016), Geochemical evidence in the northeast Lau Basin for subduction of the Cook-Austral volcanic chain in the Tonga Trench, *Geochem. Geophys. Geosyst.*, *17*, 1694–1724, doi:10.1002/2015GC006237.

Price, R. C., and L. W. Kroenke (1991), Tectonics and magma genesis in the northern North Fiji Basin, *Mar. Geol.*, *98*(2), 241–258.

Putirka, K. (2008), Excess temperatures at ocean islands: Implications for mantle layering and convection, *Geology*, *36*(4), 283–286.

Regelous, M., S. Turner, T. J. Falloon, P. Taylor, J. Gamble, and T. Green (2008), Mantle dynamics and mantle melting beneath Niuafo'ou Island and the northern Lau back-arc basin, *Contrib. Mineral. Petrol.*, *156*, 103–118, doi:10.1007/s00410-007-0276-7.

Resing, J. A., et al. (2011), Active submarine eruption of boninite in the northeastern Lau Basin, *Nat. Geosci.*, *4*(11), 799–806.

Ruellan, E., J. Delteil, I. Wright, and T. Matsumoto (2003), From rifting to active spreading in the Lau Basin–Havre Trough backarc system (SW Pacific): Locking/unlocking induced by seamount chain subduction, *Geochem. Geophys. Geosyst.*, *4*(5), 8909, doi:10.1029/2001GC000261.

Salters, V. J. M., and W. M. White (1998), Hf isotope constraints on mantle evolution, *Chem. Geol.*, *145*(3), 447–460.

Salters, V. J. M., S. Mallick, S. R. Hart, C. E. Langmuir, and A. Stracke (2011), Domains of depleted mantle: New evidence from hafnium and neodymium isotopes, *Geochem. Geophys. Geosyst.*, *12*, Q08001, doi:10.1029/2011GC003617.

Schiano, P., K. Burton, and B. Dupre, J.-L. Bircka, G. Guilleb, and C. J. Allègre (2001), Correlated Os-Pb-Nd-Sr isotopes in the Austral-Cook chain basalts: The nature of mantle components in plume sources, *Earth Planet. Sci. Lett.*, *186*, 527–537.

Sobolev, A. V., and L. V. Danyushevsky (1994), Petrology and geochemistry of boninites from the north termination of the Tonga Trench: Constraints on the generation conditions of primary high-Ca boninite magmas, *J. Petrol.*, *35*(5), 1183–1211

Starkey, N. A., F. M. Stuart, R. M. Ellam, J. G. Fitton, S. Basu, and L. M. Larsen (2009), Helium isotopes in early Iceland plume picrites: Constraints on the composition of high 3 He/4 He mantle, *Earth Planet. Sci. Lett.*, *277*(1), 91–100.

Stuart, F. M., S. Lass-Evans, J. G. Fitton, and R. M. Ellam (2003), High 3He/4He ratios in picritic basalts from Baffin Island and the role of a mixed reservoir in mantle plumes, *Nature*, *424*(6944), 57–59.

Tanaka, T., et al. (2000), JNdi-1: A neodymium isotopic reference in consistency with LaJolla neodymium, *Chem. Geol.*, *168*, 279–281.

Tatsumi, Y., K. Oguri, G. Shimoda, T. Kogiso, and H. G. Barsczus (2000), Contrasting behavior of noble-metal elements during magmatic differentiation in basalts from the Cook Islands, Polynesia, *Geology*, *28*(2), 131–134.

Tian, L., P. R. Castillo, and J. W. Hawkins, B. B. Hannan, and A. J. Pietruszka (2008), Major and trace element and Sr–Nd isotope signatures of lavas from the Central Lau Basin: Implications for the nature and influence of subduction components in the back-arc mantle, *J. Volcanol. Geotherm. Res.*, *178*, 657–670, doi:10.1016/j.jvolgeores.2008.06.039.

Tian, L., P. R. Castillo, D. R. Hilton, J. W. Hawkins, B. B. Hannan, and A. J. Pietruszka (2011), Major and trace element and Sr-Nd isotope signatures of the northern Lau Basin lavas: Implications for the composition and dynamics of the back-arc basin mantle, *J. Geophys. Res.*, *116*, B11201, doi:10.1029/2011JB008791.

Timm, C., D. Bassett, I. J. Graham, C. E. de Ronde, J. Woodhead, D. Layton-Matthews, and A. B. Watts (2013), Louisville seamount subduction and its implication on mantle flow beneath the central Tonga-Kermadec arc, *Nat. Commun.*, *4*, 1720, doi:10.1038/ncomms2702.

Todd, E., J. B. Gill, and H. Freymuth (2009), Sr-Nd-Hf-Pb isotope ratios in recent NE Lau Lavas, Abstract #V51D-1721 presented at 2009 Fall Meeting, vol. 1, 1721 pp., AGU, San Francisco, Calif.

Tollstrup, D., J. Gill, A. Kent, D. Prinkey, R. Williams, Y. Tamura, and O. Ishizuka (2010), Across-arc geochemical trends in the Izu-Bonin arc: Contributions from the subducting slab, revisited, *Geochem. Geophys. Geosyst.*, *11*, Q01X10, doi:10.1029/2009GC002847.
Turner, S., and C. Hawkesworth (1998), Using geochemistry to map mantle flow beneath the Lau Basin, *Geology*, *26*, 1019–1022.
Turner, S., J. Caulfield, T. Rushmer, M. Turner, S. Cronin, I. Smith, and H. Handley (2012), Magma evolution in the primitive, intra-oceanic Tonga arc: Rapid petrogenesis of dacites at Fonulaei volcano, *J. Petrol.*, *53*, 1231–1253.
Valbracht, P. J., T. Staudacher, A. Malahoff, and C. J. Allègre (1997), Noble gas systematics of deep rift zone glasses from Loihi Seamount, Hawaii, *Earth Planet. Sci. Lett.*, *150*, 399–411.
Vanderkluysen, L., J. J. Mahoney, A. A. Koppers, C. Beier, M. Regelous, J. S. Gee, and P. F. Lonsdale (2014), Louisville Seamount Chain: Petrogenetic processes and geochemical evolution of the mantle source, *Geochem. Geophys. Geosyst.*, *15*, 2380–2400, doi:10.1002/2014gc005288.
Vervoort, J. D., P. J. Patchett, J. Blichert-Toft, and F. Albarède (1999), Relationships between Lu-Hf and Sm-Nd isotopic systems in the global sedimentary system, *Earth Planet. Sci. Lett.*, *168*(1), 79–99.
Volpe, A. M., J. D. Macdougall, and J. W. Hawkins (1988), Lau Basin basalts (LBB): Trace element and Sr-Nd isotopic evidence for heterogeneity in backarc basin mantle, *Earth Planet. Sci. Lett.*, *90*, 174–186.
Wendt, J. I., M. Regelous, K. D. Collerson, and A. Ewart (1997), Evidence for a contribution from two mantle plumes to island-arc lavas from northern Tonga, *Geology*, *25*, 611–614.
Wessel, P., and L. W. Kroenke (2008), Pacific absolute plate motion since 145 Ma: An assessment of the fixed hot spot hypothesis, *J. Geophys. Res.*, *113*, B06101, doi:10.1029/2007JB005499.
White, W. M., and J. Patchett (1984), Hf-Nd-Sr isotopes and incompatible element abundances in island arcs'' implications for magma origins and crust-mantle evolution, *Earth Planet. Sci. Lett.*, *67*, 167–185.
Whelan, P. M., J. B. Gill, E. Kollman, R. A. Duncan, and R. E. Drake (1985), Radiometric dating of magmatic stages in Fiji, in *Geology and Offshore Resources of the Pacific Island Arcs–Tonga Region*, edited by D. W. Scholl and T. L. Vallier, pp. 415–440, Circum-Pacific Council for Energy and Resources Earth Science Series 2.
Woodhall, D. (1987), Geology of Rotuma, *Bull 8*, 29 pp., Min. Resour. Dep., Min. of Lands Energy & Min. Res., Gov. of Fiji.
Woodhead, J. D. (1996), Extreme HIMU in an oceanic setting: The geochemistry ofMangaia Island (Polynesia), and temporal evolution of the Cook-Austral hotspot, *J. Volcanol. Geotherm. Res.*, *72*(1–2), 1–19.
Workman, R. K., and S. R. Hart (2005), Major and trace element composition of the depleted MORB mantle (DMM), *Earth Planet. Sci. Lett.*, *231*, 53–72, doi:10.1029/2003GC000568.
Workman, R. K., S. R. Hart, M. G. Jackson, M. Regelous, K. A. Farley, J. Blusztajn, M. Kurz, and H. Staudigel (2004), Recycled metasomatized lithosphere as the origin of the Enriched Mantle II (EM2) end-member: Evidence from the Samoan Volcanic Chain, *Geochem. Geophys. Geosyst.*, *5*, Q04008, doi:10.1029/2003GC000623.
Wright, E., and W. M. White (1987), The origin of Samoa: New evidence from Sr, Nd, Pb isotopes, *Earth Planet. Sci. Lett.*, *81*, 151–162.